The iron-dependent repressor YtgR regulates the tryptophan salvage pathway through a bipartite mechanism of transcriptional control in *Chlamydia trachomatis*

Nick D. Pokorzynski[1], Amanda J. Brinkworth[1] and Rey A. Carabeo[1]

[1]Center for Reproductive Biology, School of Molecular Biosciences, College of Veterinary Medicine, Washington State University, Pullman, WA, USA, 99164.

Corresponding Author:

Rey A. Carabeo

1770 NE Stadium Way, Biotechnology & Life Sciences Bldg., Washington State University

Pullman, WA, 99164

(509) 335-7788

rey.carabeo@wsu.edu

Keywords: stress response, transcription, tryptophan biosynthesis, iron-dependent regulation, repression

Abstract (Word Limit:150, Word Count:150)

During infection, pathogens are starved of essential nutrients such as iron and tryptophan by host immune effectors. Without conserved global stress response regulators, how the obligate intracellular bacterium *Chlamydia trachomatis* arrives at a physiologically similar “persistent” state in response to starvation of either nutrient remains unclear. Here, we report on the iron-dependent regulation of the *trpRBA* tryptophan salvage pathway in *C. trachomatis.* Iron starvation specifically induces *trpBA* expression from a novel promoter element within an intergenic region flanked by *trpR* and *trpB*. YtgR, the only known iron-dependent regulator in *Chlamydia*, can bind to the *trpRBA* intergenic region upstream of the alternative *trpBA* promoter to repress transcription. Simultaneously, YtgR binding promotes the termination of transcripts from the primary promoter upstream of *trpR*. This is the first description of an iron-dependent mechanism regulating prokaryotic tryptophan biosynthesis that may indicate the existence of novel approaches to gene regulation and stress response in *Chlamydia.*

46 **Introduction**

47 Nutrient acquisition is critical for the success of pathogenic bacteria. Many
48 pathogenic bacteria must siphon nutrients from their hosts, such as nucleotides, amino
49 acids and biometals (Brown, Palmer, & Whiteley, 2008; Eisenreich, Dandekar,
50 Heesemann, & Goebel, 2010; Ray, Marteyn, Sansonetti, & Tang, 2009; Skaar, 2010).
51 This common feature among pathogens renders them susceptible to nutrient limitation
52 strategies associated with the host immune response (Hood & Skaar, 2012).
53 Counteractively, bacterial pathogens have evolved sophisticated molecular mechanisms
54 to respond to nutrient deprivation, involving increasingly complex and sophisticated
55 nutrient-sensing regulatory networks. These stress response mechanisms are essential
56 for pathogens to avoid clearance by the immune system. By delineating their function at
57 the molecular level, we can better target aspects of the host-pathogen interface suitable
58 for therapeutic manipulation. However, stress responses in the obligate intracellular
59 bacterium *Chlamydia trachomatis* are relatively poorly characterized, leaving
60 unanswered many fundamental questions about the biology of this pathogen.

61 *Chlamydia trachomatis* is the leading cause of bacterial sexually transmitted
62 infections (STIs) and infection-derived preventable blindness worldwide (CDC, 2017;
63 Newman et al., 2015; H. R. Taylor, Burton, Haddad, West, & Wright, 2014). Genital
64 infections of chlamydia disproportionately affect women and are associated with serious
65 sequelae in the female reproductive tract such as tubal factor infertility (Hafner, 2015).
66 Chlamydiae are Gram-negative bacterial parasites that develop within a pathogen-
67 specified membrane-bound organelle termed the inclusion (Moore & Ouellette, 2014).
68 Chlamydial development is uniquely characterized by a biphasic interconversion of an

69 infectious elementary body (EB) with a non-infectious, but replicative reticulate body
70 (RB) (AbdelRahman & Belland, 2005). An obligate intracellular lifestyle has led to
71 reductive genome evolution across chlamydial species; Chlamydiae have retained
72 genes uniquely required for their survival, but have become nutritionally dependent on
73 their hosts by discarding many metabolism-related genes (Clarke, 2011). Of note, *C.*
74 *trachomatis* does not possess genes necessary for eliciting a stringent response to
75 nutrient starvation (*e.g. relA, spoT*), suggesting that this pathogen may utilize novel
76 mechanisms to respond to nutrient stress (Stephens et al., 1998).

77 It is well established that in response to various stressors, Chlamydiae deviate
78 from their normal developmental program to initiate an aberrant developmental state,
79 termed "persistence" (Wyrick, 2010). This persistent state is distinguished by the
80 presence of viable, but non-cultivable, abnormally enlarged chlamydial organisms that
81 display dysregulated gene expression. Importantly, *Chlamydia* can be reactivated from
82 persistence by abatement of the stress condition. As such, chlamydial persistence at
83 least superficially resembles a global stress response mechanism. Yet the molecular
84 underpinnings of this phenotype are poorly understood, with most published studies
85 focusing on the molecular and metabolic character of the aberrant, persistent form. It is
86 therefore unclear to what extent primary stress responses contribute to the global
87 persistent phenotype in *Chlamydia*.

88 The best described inducer of persistence is the pro-inflammatory cytokine
89 interferon-gamma (IFN-γ). The bacteriostatic effect of IFN-γ has been primarily
90 attributed to host cell tryptophan (Trp) catabolism, an amino acid for which *C.*
91 *trachomatis* is auxotrophic (Byrne, Lehmann, & Landry, 1986; Fehlner-Gardiner et al.,

92 2002; M. W. Taylor & Feng, 1991). Following IFN-γ stimulation, infected host cells up-
93 regulate expression of indoleamine-2,3-dioxygenase (IDO1), which catabolizes Trp to
94 *N*-formylkynurenine via cleavage of the indole ring (Macchiarulo, Camaioni, Nuti, &
95 Pellicciari, 2009). *C. trachomatis* cannot recycle kynurenines, unlike some other
96 chlamydial species (Wood, Roshick, & McClarty, 2004), and thus IFN-γ stimulation
97 effectively results in Trp starvation to *C. trachomatis*. The primary regulatory response
98 to Trp starvation in *C. trachomatis* is mediated by a TrpR ortholog, whose Trp-
99 dependent binding to cognate promoter elements represses transcription (Akers & Tan,
100 2006; Carlson, Wood, Roshick, Caldwell, & McClarty, 2006). This mechanism of
101 regulatory control is presumably limited in *C. trachomatis*, as homologs of genes
102 regulated by TrpR in other bacteria (*e.g. trpF, aroH, aroL*) have not been shown to
103 respond to Trp limitation (Wood et al., 2003).
104 In many Gram-negative bacteria, such as *Escherichia coli*, *trpR* is monocistronic
105 and distal to the Trp biosynthetic operon. In *C. trachomatis,* TrpR is encoded in an
106 operon, *trpRBA*, which also contains the Trp synthase α- and β- subunits (TrpA and
107 TrpB, respectively), and possesses a 351 base-pair (bp) intergenic region (IGR) that
108 separates *trpR* from *trpBA*. The functional significance of the *trpRBA* IGR is poorly
109 characterized. While a putative TrpR operator sequence was identified in the IGR
110 overlapping an alternative transcriptional origin for *trpBA* (Carlson et al., 2006), TrpR
111 binding was not shown (Akers & Tan, 2006). Based on *in silico* predictions, an
112 attenuator sequence has been annotated within the *trpRBA* IGR (Merino & Yanofsky,
113 2005), but this has not been thoroughly validated experimentally. Regardless, the IGR is
114 >99% conserved at the nucleotide sequence level across ocular, genital and

115 lymphogranuloma venereum (LGV) serovars of *C. trachomatis*, indicating functional
116 importance (Carlson, Porcella, Mcclarty, & Caldwell, 2005; Seth-Smith et al., 2009;
117 Stephens et al., 1998; Thomson et al., 2008). Therefore, outside of TrpR-mediated
118 repression, the complete detail of *trpRBA* regulation remains poorly elucidated and
119 previous reports have indicated the possibility of more complex mechanisms of
120 regulation (Brinkworth, Wildung, & Carabeo, 2018).

121 In evaluating alternative regulatory modes of the *trpRBA* operon, an interesting
122 consideration is the pleiotropic effects induced by IFN-γ stimulation of infected cells.
123 IFN-γ is involved in many processes that limit iron and other essential biometals to
124 intracellular pathogens as a component of host nutritional immunity (Cassat & Skaar,
125 2013; Hood & Skaar, 2012). *Chlamydia* have a strict iron dependence for normal
126 development, evidenced by the onset of persistence following prolonged iron limitation
127 (Raulston, 1997). Importantly, *Chlamydia* presumably acquire iron via vesicular
128 interactions between the chlamydial inclusion and slow-recycling transferrin (Tf)-
129 containing endosomes (Ouellette & Carabeo, 2010). IFN-γ is known to down-regulate
130 transferrin receptor (TfR) expression in both monocytes and epithelial cells with
131 replicative consequences for resident intracellular bacteria (T. F. Byrd & Horwitz, 1993;
132 T. Byrd & Horwitz, 1989; Igietseme, Ananaba, Candal, Lyn, & Black, 1998; Nairz et al.,
133 2008). However, iron homeostasis in *Chlamydia* is poorly understood due to the lack of
134 functionally characterized homologs to iron acquisition machinery that are highly
135 conserved in other bacteria (Pokorzynski, Thompson, & Carabeo, 2017). Only the
136 *ytgABCD* operon, encoding a metal permease, has been clearly linked to iron
137 acquisition (J. D. Miller, Sal, Schell, Whittimore, & Raulston, 2009). Intriguingly, the

138 YtgC (CTL0325) open reading frame (ORF) encodes a N-terminal permease domain
139 fused to a C-terminal DtxR-like repressor domain, annotated YtgR (Akers, HoDac,
140 Lathrop, & Tan, 2011; Thompson, Nicod, Malcolm, Grieshaber, & Carabeo, 2012). YtgR
141 is cleaved from the permease domain during infection and functions as an iron-
142 dependent transcriptional repressor to autoregulate the expression of its own operon
143 (Thompson et al., 2012). YtgR represents the only identified iron-dependent
144 transcriptional regulator in *Chlamydia.* Whether YtgR maintains a more diverse
145 transcriptional regulon beyond the *ytgABCD* operon has not yet been addressed and
146 remains an intriguing question in the context of immune-mediated iron limitation to *C.*
147 *trachomatis*.
148 Consistent with the highly reduced capacity of the chlamydial genome, it is likely
149 that *C. trachomatis* has a limited ability to tailor a specific response to each individual
150 stress. In the absence of identifiable homologs for most global stress response
151 regulators in *C. trachomatis*, we hypothesized that primary stress responses to
152 pleiotropic insults may involve mechanisms of regulatory integration, whereby important
153 molecular pathways are co-regulated by stress-responsive transcription factors such
154 that they can be utilized across multiple host-mediated stresses. Here, we report on the
155 unique iron-dependent regulation of the *trpRBA* operon in *Chlamydia trachomatis.* We
156 propose a model of iron-dependent transcriptional regulation of *trpRBA* mediated by the
157 repressor YtgR binding specifically to the IGR, which may have implications for how *C.*
158 *trachomatis* responds to immunological and environmental insults. Such a mechanism
159 of iron-dependent regulation of Trp biosynthesis has not been previously described in
160 any other prokaryote and adds to the catalog of regulatory models for Trp biosynthetic

161 operons in bacteria. Further, it reveals a highly dynamic mode of regulatory integration
162 within the *trpRBA* operon, employing bipartite control at the transcription initiation and
163 termination steps.

164 **Results**

165 **Brief iron limitation via 2,2-bipyridyl treatment yields iron-starved, but non-**
166 **persistent *Chlamydia trachomatis.*** To identify possible instances of regulatory
167 integration between iron and Trp starvation in *C. trachomatis*, we optimized a stress
168 response condition that preceded the development of a characteristically persistent
169 phenotype. We reasoned that in order to effectively identify regulatory integration, we
170 would need to investigate the bacterium under stressed, but not aberrant, growth
171 conditions such that we could distinguish primary stress responses from abnormal
172 growth. To specifically investigate the possible contribution of iron limitation to a broader
173 immunological (*e.g.* IFN-γ-mediated) stress, we utilized the membrane-permeable iron
174 chelator 2,2-bipyridyl (Bpdl), which has the advantage of rapidly and homogeneously
175 starving *C. trachomatis* of iron (Thompson & Carabeo, 2011). We chose to starve *C.*
176 *trachomatis* serovar L2 of iron starting at 12 hrs post-infection (hpi), or roughly at the
177 beginning of mid-cycle growth. At this point the chlamydial organisms represent a
178 uniform population of replicative RBs that are fully competent, both transcriptionally and
179 translationally, to respond to stress. We treated infected HeLa cell cultures with 100 μM
180 Bpdl or mock for either 6 or 12 hours (hrs) to determine a condition sufficient to limit iron
181 to *C. trachomatis* without inducing hallmark persistent phenotypes. We stained infected
182 cells seeded on glass coverslips with convalescent human sera and analyzed
183 chlamydial inclusion morphology under both Bpdl- and mock-treated conditions by laser

184 point-scanning confocal microscopy (Figure 1A). Following 6 hrs of Bpdl treatment,
185 chlamydial inclusions were largely indistinguishable from mock-treated inclusions,
186 containing a homogeneous population of larger organisms, consistent with RBs in mid-
187 cycle growth. However, by 12 hrs of Bpdl treatment, the inclusions began to display
188 signs of aberrant growth: they were perceptibly smaller, more comparable in size to 18
189 hpi, and contained noticeably fewer organisms, perhaps indicating a delay in RB-to-EB
190 differentiation. These observations were consistent with our subsequent analysis of
191 genome replication by quantitative PCR (qPCR; Figure 1B.) At 6 hrs of Bpdl treatment,
192 there was no statistically distinguishable difference in genome copy number when
193 compared to the equivalent mock-treated time-point. However, by 12 hrs of treatment,
194 genome copy number was significantly reduced 4.7-fold in the Bpdl-treated group
195 relative to mock-treatment (p = 0.0033). We then assayed the transcript expression of
196 two markers for persistence by reverse transcription quantitative PCR (RT-qPCR): the
197 early gene *euo*, encoding a transcriptional repressor of late-cycle genes (Figure 1C),
198 and the adhesin *omcB,* which is expressed late in the developmental cycle (Figure 1D).
199 Characteristic persistence would display elevated *euo* expression late into infection, and
200 suppressed *omcB* expression throughout development. We observed that at 6 hrs of
201 Bpdl treatment, there was no statistically distinguishable difference in either *euo* or
202 *omcB* expression when compared to the mock-treatment. Still at 12 hrs of Bpdl
203 treatment, *euo* expression was unchanged. However, *omcB* expression was
204 significantly induced following 12 hrs of Bpdl-treatment (p = 0.00015). This was
205 unexpected, but we note that *omcB* expression has been shown to vary between
206 chlamydial serovars and species when starved for iron (Pokorzynski et al., 2017).

207 Collectively, these data indicated that 6 hrs of Bpdl treatment was a more suitable time-
208 point at which to monitor iron-limited stress responses.
209 We additionally assayed these same metrics following 6 or 12 hrs of Trp
210 starvation by culturing cells in either Trp-replete or Trp-deplete DMEM-F12 media
211 supplemented with fetal bovine serum (FBS) pre-dialyzed to remove amino acids. We
212 observed no discernable change in inclusion morphology out to 12 hrs of Trp starvation
213 (Figure 1 – Figure Supplement 1A), but genome copy numbers were significantly
214 reduced 2.7-fold at this time-point (p = 0.00612; Figure 1 – Figure Supplement 1B). The
215 transcript expression of *euo* (Figure 1 – Figure Supplement 1C) and *omcB* (Figure 1 –
216 Figure Supplement 1D) did not significantly change at either treatment duration, but Trp-
217 depletion did result in a 2.0-fold reduction in *omcB* expression, consistent with a more
218 characteristic persistent phenotype. These data therefore also indicated that 6 hrs of
219 treatment would be ideal to monitor non-persistent responses to Trp limitation.
220
221
222
223
224
225
226

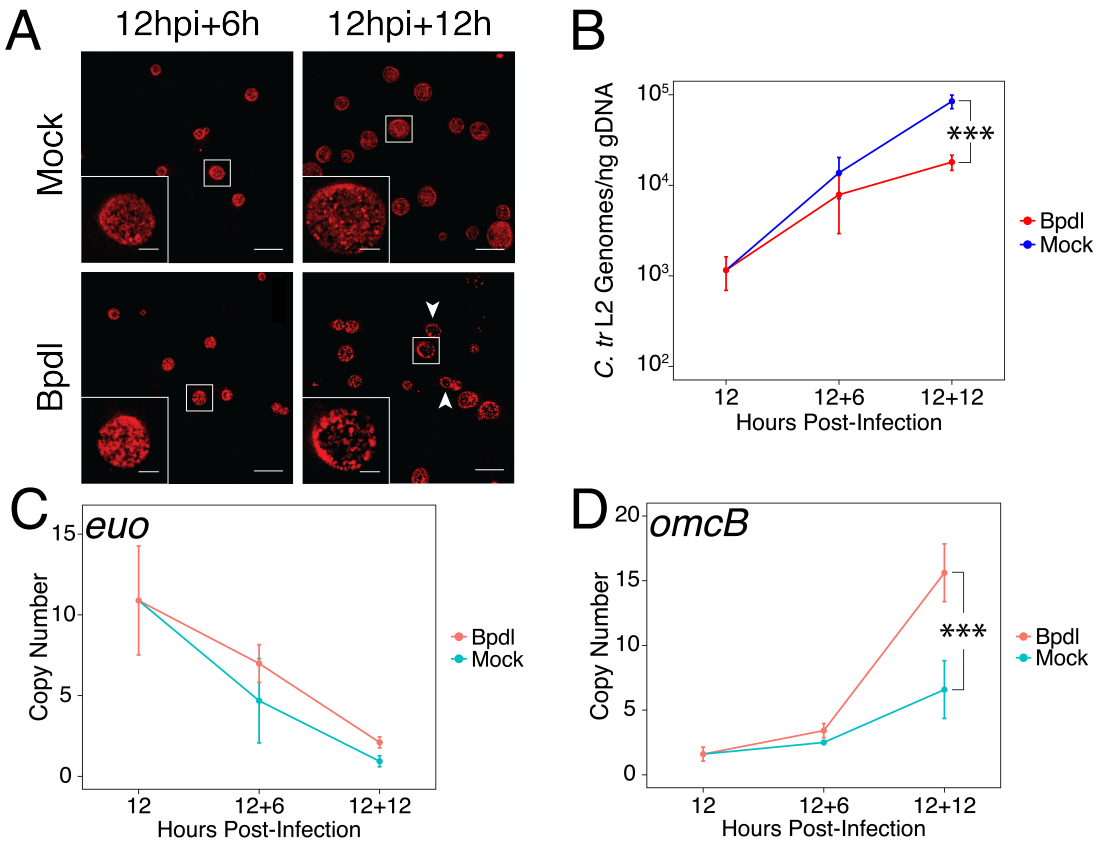

Figure 1. Brief iron limitation via 2,2-bipyridyl treatment precedes the onset of characteristic chlamydial persistence. (*A*) *C. trachomatis* L2-infected HeLa cells were fixed and stained with convalescent human sera to image inclusion morphology by confocal microscopy following Bpdl treatment at the indicated times post-infection. Arrowheads indicate inclusions with visibly fewer organisms in the 12-hour Bpdl-treated condition. Figure shows representative experiment of three biological replicates. Scale bar = 25 μm, Inset scale bar = 5 μm. (*B*) Genomic DNA (gDNA) was harvested from infected HeLa cells at the indicated times post-infection under iron-replete (blue) and -deplete (red) conditions. Chlamydial genome copy number was quantified by qPCR. Chlamydial genome replication is stalled following 12 hours of Bpdl treatment, but not 6. N=2. (*C*) Total RNA was harvested from infected HeLa cells at the indicated times post-infection under iron-replete (teal) and -deplete (orange) conditions. The transcript abundance of hallmark persistence genes *euo* and (*D*) *omcB* were quantified by RT-qPCR and normalized against genome copy number. Only at 12 hours of Bpdl treatment is *omcB* expression significantly affected. N=3 for 12+6, N=2 for 12+12. Statistical significance was determined by One-Way ANOVA followed by post-hoc pairwise *t*-tests with Bonferroni's correction for multiple comparisons. * = $p < 0.05$, ** = $p < 0.01$, *** = $p < 0.005$.

258 We next sought to determine whether our brief 6-hr Bpdl treatment was sufficient
259 to elicit a transcriptional iron starvation phenotype. We chose to analyze the expression
260 of three previously identified iron-regulated transcripts, *ytgA* (Figure 2A), *ahpC* (Figure
261 2B) and *devB* (Figure 2C), by RT-qPCR under Bpdl- and mock-treated conditions (Dill,
262 Dessus-Babus, & Raulston, 2009; Thompson & Carabeo, 2011). In addition, we
263 analyzed the expression of one non-iron-regulated transcript, *dnaB* (Figure 2D), as a
264 negative control (Brinkworth et al., 2018). Following 6 hrs of Bpdl treatment, we
265 observed that the transcript expression of the periplasmic iron-binding protein *ytgA* was
266 significantly elevated 1.75-fold relative to the equivalent mock-treated time-point (p =
267 0.0052). However, we did not observe induction of *ytgA* transcript expression relative to
268 the 12 hpi time-point. We distinguish here between *elevated* and *induced* transcript
269 expression, as chlamydial gene expression is highly developmentally regulated. Thus, it
270 can be more informative to monitor longitudinal expression of genes, *i.e.* their induction,
271 as opposed to elevation relative to an equivalent control time-point, which may simply
272 represent a stall in development. While we did not observe induction of *ytgA*, which
273 would be more consistent with an iron-starved phenotype, we reason that this is a
274 consequence of the brief treatment period, and that longer iron starvation would
275 produce a more robust induction of iron-regulated transcripts. Note that the identification
276 of *ytgA* as iron-regulated has only been previously observed following extended periods
277 of iron chelation (J. D. Miller et al., 2009; Raulston et al., 2007; Thompson & Carabeo,
278 2011). Similarly, we observed that the transcript expression of the thioredoxin *ahpC* was
279 significantly elevated 2.15-fold relative to the equivalent mock-treated time-point (p =
280 0.038) but was not induced relative to the 12 hpi time-point. The transcript expression of

281 *devB*, encoding a 6-phosphogluconolactonase involved in the pentose phosphate
282 pathway, was not observed to significantly respond to our brief iron limitation condition,
283 suggesting that it is not a component of the primary iron starvation stress response in *C.*
284 *trachomatis.* As expected, the transcript expression of *dnaB*, a replicative DNA helicase,
285 was not altered by our iron starvation condition, consistent with its presumably iron-
286 independent regulation (Brinkworth et al., 2018). Overall, these data confirmed that our
287 6-hr Bpdl treatment condition was suitable to produce a mild iron starvation phenotype
288 at the transcriptional level, thus facilitating our investigation of iron-dependent regulatory
289 integration.
290
291
292
293
294
295
296
297
298
299
300
301
302

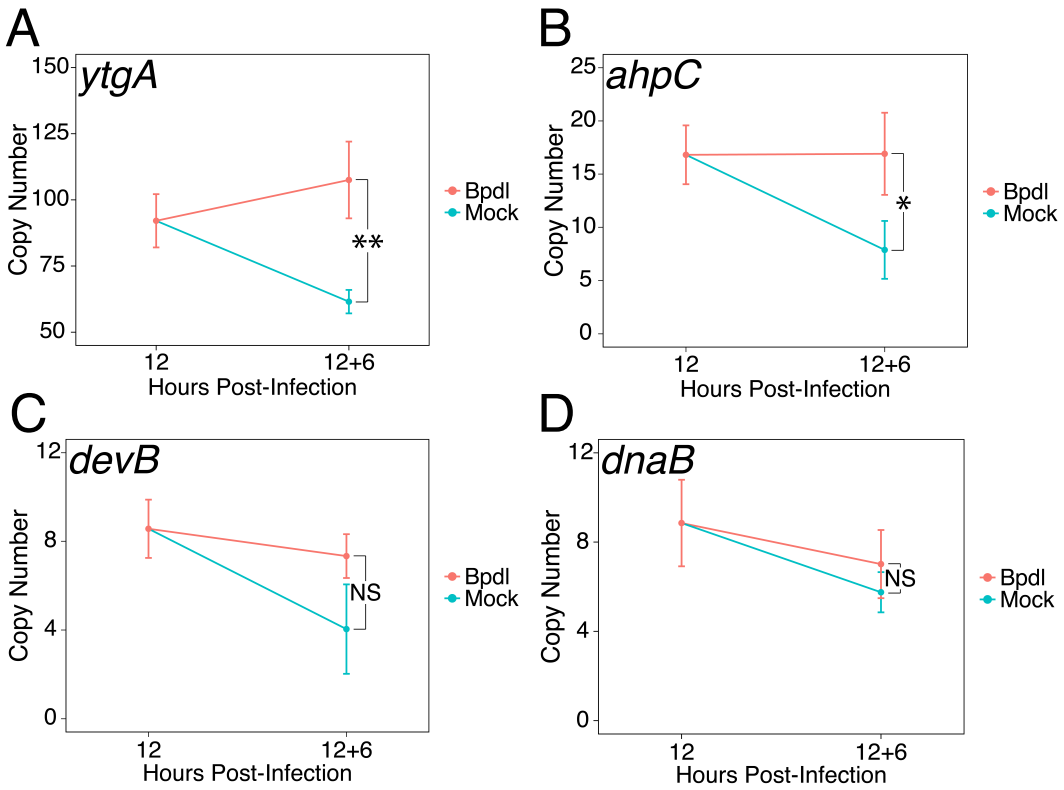

Figure 2. Brief iron limitation condition produces mild iron-starved transcriptional phenotype. (*A*) Total RNA and gDNA was harvested from infected HeLa cells at the indicated times post-infection under iron-replete (teal) and -deplete (orange) conditions. The transcript abundance of iron-regulated *ytgA,* (*B*) *ahpC,* (*C*) *devB* and (*D*) non-iron regulated *dnaB* were quantified by RT-qPCR and normalized against genome copy number. The transcript expression of *ytgA* and *ahpC* were significantly elevated following 6-hour Bpdl treatment, indicative or iron starvation to *C. trachomatis.* N=3. Statistical significance was determined by One-Way ANOVA followed by post-hoc pairwise *t*-tests with Bonferroni's correction for multiple comparisons. * = $p < 0.05$, ** = $p < 0.01$, *** = $p < 0.005$.

331 **Transcript expression of the *trpRBA* operon is differentially regulated by iron in**
332 ***Chlamydia trachomatis.*** Upon identifying an iron limitation condition that produced a
333 relevant transcriptional phenotype while avoiding the onset of persistent development,
334 we aimed to investigate whether the immediate response to iron starvation in *C.*
335 *trachomatis* would result in the consistent induction of pathways unrelated to iron
336 utilization/acquisition, but nevertheless important for surviving immunological stress.
337 The truncated Trp biosynthetic operon, *trpRBA* (Figure 3A), has been repeatedly linked
338 to the ability of genital and LGV serovars (D-K and L1-3, respectively) of *C. trachomatis*
339 to counter IFN-γ-mediated stress. This is due to the capacity of the chlamydial Trp
340 synthase in these serovars to catalyze the β synthase reaction, *i.e.* the condensation of
341 indole to the amino acid serine to form Trp (Fehlner-Gardiner et al., 2002). In the
342 presence of exogenous indole, *C. trachomatis* is therefore able to biosynthesize Trp
343 such that it can prevent the development of IFN-γ-mediated persistence.
344 Correspondingly, the expression of *trpRBA* is highly induced following IFN-γ stimulation
345 of infected cells (Belland et al., 2003; Østergaard et al., 2016). These data have
346 historically implicated Trp starvation as the primary mechanism by which persistence
347 develops in *C. trachomatis* following exposure to IFN-γ. However, these studies have
348 routinely depended on prolonged treatment conditions that monitor the terminal effect of
349 persistent development, as opposed to the immediate molecular events which may
350 have important roles in the developmental fate of *Chlamydia.* As such, these studies
351 may have missed the contribution of other IFN-γ-stimulated insults such as iron
352 limitation.

353 To decouple Trp limitation from iron limitation and assess their relative
354 contribution to regulating a critical pathway for responding to IFN-γ-mediated stress, we
355 monitored the transcript expression of the *trpRBA* operon under brief Trp or iron
356 starvation by RT-qPCR. When starved for Trp for 6 hrs, we observed that the
357 expression of *trpR*, *trpB* and *trpA* were all significantly induced greater than 10.5-fold
358 relative to 12 hpi (p = 0.00077, 0.025 and 9.7e-5, respectively; Figure 3B). All three
359 ORFs were also significantly elevated relative to the equivalent mock-treated time-point
360 (p = 0.00076, 0.025 and 9.7e-5, respectively). This result was surprising with respect to
361 the relative immediacy of operon induction in response to our Trp starvation protocol,
362 confirming the relevant Trp-starved transcriptional phenotype. To induce Trp-deprived
363 persistence in *C. trachomatis*, many laboratories rely on compounded techniques of
364 IFN-γ pre-treatment to deplete host Trp pools in conjunction with culturing in Trp-
365 depleted media, among other strategies. While the phenotypic end-point differs here, it
366 is nonetheless interesting to note that only 6 hrs of media replacement is sufficient to
367 markedly up-regulate *trpRBA* expression. This suggests that *C. trachomatis* has a
368 highly attuned sensitivity to even moderate changes in Trp levels.
369 We next performed the same RT-qPCR analysis on the expression of the *trpRBA*
370 operon in response to 6 hrs of iron limitation via BpdI treatment (Figure 3C). While we
371 observed that the transcript expression of all three ORFs was significantly elevated at
372 least 2.1-fold relative to the equivalent mock-treated time-point (p = 0.015, 0.00098 and
373 0.0062, respectively), we made the intriguing observation that only the expression of
374 *trpB* and *trpA* was significantly induced relative to 12 hpi (p = 0.00383 and 0.0195,
375 respectively). The significant induction of *trpBA* expression, but not *trpR* expression,

suggested that *trpBA* are specifically regulated by iron availability. This result is consistent with a recent survey of the iron-regulated transcriptome in *C. trachomatis* by RNA-Sequencing, which also reported that iron-starved *Chlamydia* specifically up-regulate *trpBA* expression in the absence of altered *trpR* expression (Brinkworth et al., 2018). Our results expand on this finding by providing a more detailed investigation into the specific profile of this differential regulation of *trpRBA* in response to iron deprivation. Taken together, these findings demonstrate that an important stress response pathway, the *trpRBA* operon, is regulated by the availability of both Trp and iron, consistent with the notion that the pathway may be cooperatively regulated to respond to various stress conditions. Notably, iron-dependent regulation of Trp biosynthesis has not been previously documented in other prokaryotes.

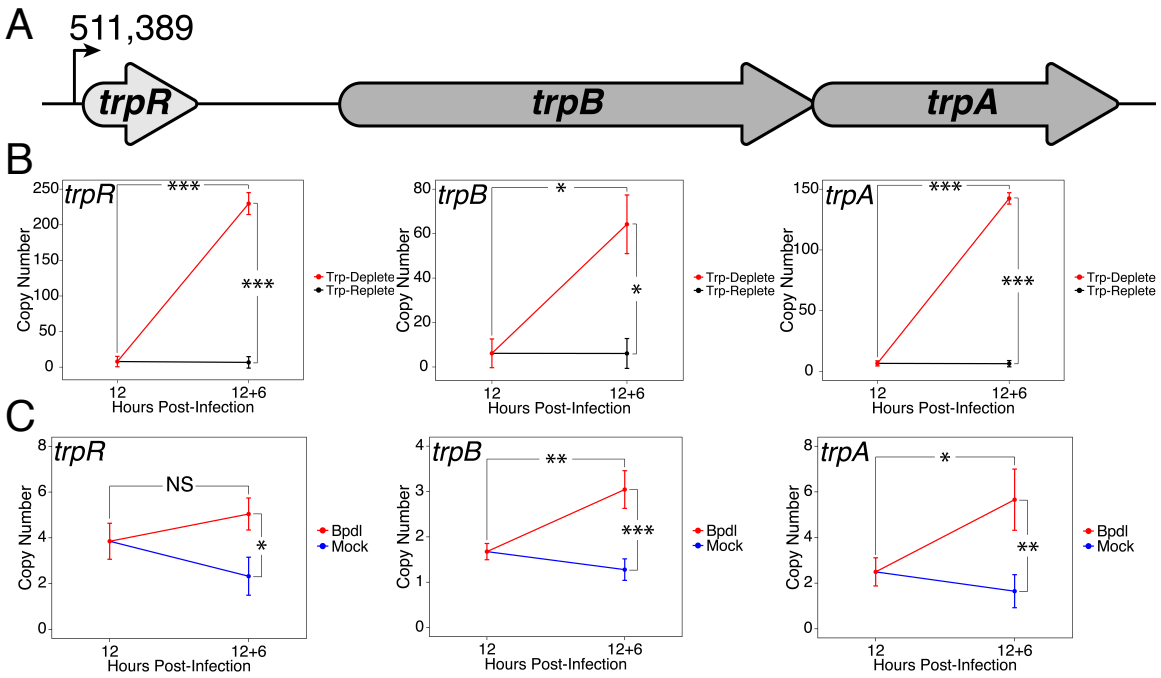

Figure 3. Expression of the *trpRBA* operon in *C. trachomatis* is differentially regulated by brief iron limitation. (*A*) Cartoon depiction of the *trpRBA* operon (drawn to scale) with the primary transcriptional start site upstream of *trpR* annotated. (*B*) Total RNA and gDNA were harvested from infected HeLa cells at the indicated times post-infection under Trp-replete (black) and -deplete (red) conditions. The transcript expression of *trpRBA* operon was quantified by RT-qPCR and normalized against genome copy number. All three ORFs are significantly induced relative to 12 hpi following Trp starvation. N=2. (*C*) Total RNA and gDNA were harvested from infected HeLa cells at the indicated times post-infection under iron-replete (blue) and -deplete (red) conditions. The transcript expression of *trpRBA* operon was quantified by RT-qPCR and normalized against genome copy number. Only *trpB* and *trpA* expression was significantly induced relative to 12 hpi. N=3. Statistical significance was determined by One-Way ANOVA followed by post-hoc pairwise *t*-tests with Bonferroni's correction for multiple comparisons. * = $p < 0.05$, ** = $p < 0.01$, *** = $p < 0.005$.

429 **Specific iron-regulated expression of *trpBA* originates from a novel alternative**
430 **transcriptional start site within the *trpRBA* intergenic region.** We hypothesized that
431 the specific iron-related induction of *trpBA* expression relative to *trpR* expression may
432 be attributable to an iron-regulated alternative transcriptional start site (alt. TSS)
433 downstream of the *trpR* ORF. Indeed, a previous study reported the presence of an alt.
434 TSS in the *trpRBA* IGR, located 214 nucleotides upstream of the *trpB* translation start
435 position (Carlson et al., 2006). However, a parallel study could not identify a TrpR
436 binding site in the *trpRBA* IGR (Akers & Tan, 2006). We reasoned that a similar alt. TSS
437 may exist in the IGR that controlled the iron-dependent expression of *trpBA.* We
438 therefore performed Rapid Amplification of 5'-cDNA Ends (5'-RACE) on RNA isolated
439 from *C. trachomatis* L2-infected HeLa cells using the SMARTer 5'/3' RACE Kit workflow
440 (Takara Bio). Given the low expression of the *trpRBA* operon during normal
441 development, we utilized two sequential gene-specific amplification steps (nested 5'-
442 RACE) to identify 5' cDNA ends in the *trpRBA* operon. These nested RACE conditions
443 resulted in amplification that was specific to infected-cells (Figure 4 – Figure
444 Supplement 1A). Using this approach, we analyzed four conditions: 12 hpi, 18 hpi, 12
445 hpi + 6 hrs of Bpdl treatment, and 12 hpi + 6 hrs of Trp-depletion (Figure 4A). We
446 observed three RACE products that migrated with an apparent size of 1.5, 1.1 and 1.0
447 kilobases (kb). At 12 and 18 hpi, all three RACE products exhibited low abundance,
448 even following the nested PCR amplification. This observation was consistent with the
449 expectation that the expression of the *trpRBA* operon is very low under normal, iron and
450 Trp-replete conditions. However, we note that the 6-hr difference in development did
451 appear to alter the representation of the 5' cDNA ends, which may suggest a stage-

452 specific promoter utilization within the *trpRBA* operon. In our Trp starvation condition,
453 we observed an apparent increase in the abundance of the 1.5 kb RACE product, which
454 was therefore presumed to represent the primary TSS upstream of *trpR*, at nucleotide
455 position 511,389 (*C. trachomatis* L2 434/Bu). Interestingly, the 1.0 kb product displayed
456 a very similar apparent enrichment following BpdI treatment, suggesting that this RACE
457 product represented a specifically iron-regulated TSS. Both the 1.5 and 1.0 kb RACE
458 products were detectable in the Trp-depleted and iron-depleted conditions, respectively,
459 during the primary RACE amplification, consistent with their induction under these
460 conditions (Figure 4 – Figure Supplement 1B).

461 If iron depletion was inducing *trpBA* expression independent of *trpR,* we
462 reasoned that we would observe specific enrichment of *trpB* sequences in our 5'-RACE
463 cDNA samples relative to *trpR* sequences. We again utilized RT-qPCR to quantify the
464 abundance of *trpB* transcripts relative to *trpR* transcripts in the 5'-RACE total RNA
465 samples (Figure 4B). In agreement with our model, only under iron starved conditions
466 did we observe a significant enrichment of *trpB* relative to *trpR* ($p < 0.01$). Additionally,
467 we observed that at 12 and 18 hpi in iron-replete conditions, the ratio of *trpB* to *trpR* was
468 approximately 1.0, suggesting non-preferential basal expression across the three
469 putative TSSs. Another factor contributing to this ratio is the synthesis of the full-length
470 *trpRBA* polycistron. In support of this, the *trpB* to *trpR* ratio remained near 1.0 under the
471 Trp-starved condition, which would be expected during transcription read-through of the
472 whole operon. The apparent lack of preferential promoter utilization as described above
473 could be attributed to the relatively low basal expression of the operon at 12 and 18 hpi

474 under Trp- and iron-replete conditions, thus precluding quantitative detection of
475 differential promoter utilization in this assay.
476 To determine the specific location of the 5' cDNA ends within the *trpRBA* operon,
477 we isolated the 5'-RACE products across all conditions by gel extraction and cloned the
478 products into the pRACE vector supplied by the manufacturer. We then sequenced the
479 ligated inserts and BLASTed the sequences against the *C. trachomatis* L2 434/Bu
480 genome to identify the location of the 5'-most nucleotides (Figure 4C). These data are
481 displayed as a statistical approximation of the genomic regions most likely to be
482 represented by the respective 5'-RACE products in both histogram (semi-continuous)
483 and density plot (continuous) format (See Supplementary File 1 for a description of all
484 mapped 5'-RACE products). As expected, the 1.5 kb product mapped in a distinct and
485 tightly grouped peak near the previously annotated *trpR* TSS, with the mean and modal
486 nucleotide being 511,388 and 511,389, respectively (Figure 4 – Figure Supplement 2A).
487 Surprisingly, we found that neither the 1.1 or 1.0 kb RACE product mapped to the
488 previously reported alt. TSS in the *trpRBA* IGR, at position 511,826. Instead, we
489 observed that the 1.1 kb product mapped on average to nucleotide position 511,878,
490 with the modal nucleotide being found at 511,898 (Figure 4 – Figure Supplement 2B).
491 The 1.0 kb product mapped with a mean nucleotide position of 512,013, with the modal
492 nucleotide being 512,005 (Figure 4 – Figure Supplement 2C), only 35 bases upstream
493 of the *trpB* coding sequence. Interestingly, the 1.0 kb product mapped to a region of the
494 *trpRBA* IGR flanked by consensus σ^{66} -10 and -35 promoter elements, found at
495 positions 512,020-5 and 511,992-7, respectively (Ricci, Ratti, & Scarlato, 1995). These
496 data collectively pointed toward the 1.0 kb 5'-RACE product representing a novel, iron-

497 regulated alt. TSS and *bona fide* σ^{66}-dependent promoter element that allows for the

498 specific iron-dependent expression of *trpBA*.

499

500

501

502

503

504

505

506

507

508

509

510

511

512

513

514

515

516

517

518

519

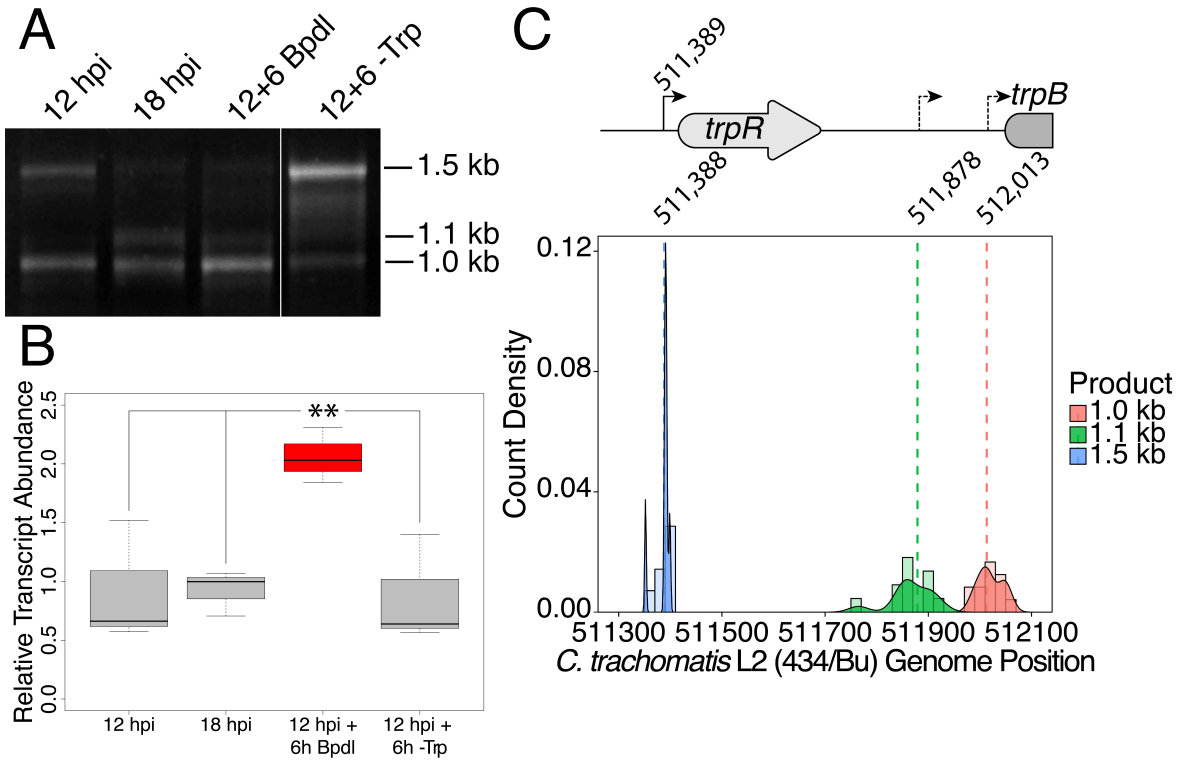

Figure 4. Iron-dependent induction of *trpBA* expression initiates within the *trpRBA* intergenic region from a novel alternative transcriptional start site. (*A*) Total RNA was harvested from infected HeLa cells at the indicated times post-infection to examine iron-dependent and Trp-dependent changes in the 5'-cDNA profile of the *trpRBA* operon by Rapid Amplification of 5' cDNA Ends (5'-RACE). RACE products were separated on an agarose gel, revealing three distinct and specific bands with apparent sizes of 1.5, 1.1 and 1.0 kb. Trp depletion led to the apparent enrichment of the 1.5 kb product, while BpdI treatment produced a similarly enriched 1.0 kb RACE product. Figure shows representative experiment of three biological replicates. (*B*) To confirm that iron-dependent induction of *trpBA* could originate from alternative transcription initiation, RT-qPCR was performed on 5'-RACE total RNA to quantify the abundance of *trpB* transcripts relative to *trpR.* Only under iron-limited conditions were *trpB* transcripts enriched relative to *trpR*. N=3. Statistical significance determined by One-way ANOVA followed by post-hoc pairwise *t*-tests. * = $p < 0.05$, ** = $p < 0.01$, *** = $p < 0.005$. (*C*) The nucleotide position of the 5' cDNA ends generated from RACE were mapped to the *C. trachomatis* L2 434/Bu genome by nucleotide BLAST. Figure displays histogram (semi-continuous; bin width=20) and overlaid density plot (continuous) distribution of 5' nucleotide positions generated from each 5'-RACE product. The dotted line represents the weighted mean of the distribution, as indicated by the integer value above each line. The identified alt. TSSs are depicted on the *trpRBA* operon (drawn to scale) above the plot. N=3.

553 **YtgR specifically binds to the *trpRBA* intergenic region in an operator-dependent**
554 **manner to repress transcription of *trpBA*.** As the only known iron-dependent
555 transcriptional regulator in *Chlamydia*, we hypothesized that YtgR may regulate the iron-
556 dependent expression of *trpBA* from the putative promoter element we characterized by
557 5'-RACE. Using bioinformatic sequence analysis, we investigated whether the *trpRBA*
558 IGR contained a candidate YtgR operator sequence. By local sequence alignment of
559 the putative YtgR operator sequence (Akers et al., 2011) and the *trpRBA* IGR, we
560 identified a high-identity alignment (76.9% identity) covering 67% of the putative
561 operator sequence (Figure 5A). Interestingly, this alignment mapped to the previously
562 identified palindrome suspected to have operator functionality (Carlson et al., 2006). By
563 global sequence alignment of the YtgR operator to the palindromic sequence, an
564 alignment identical to the local alignment was observed, which still displayed relatively
565 high sequence identity (43.5% identity). We hypothesized that this sequence functioned
566 as an YtgR operator, despite being located 184 bp upstream of the *trpBA* alt. TSS.
567 To investigate the ability of YtgR to bind and repress transcription from the
568 putative *trpBA* promoter, we implemented a heterologous two-plasmid assay that
569 reports on YtgR repressor activity as a function of β-galactosidase expression
570 (Thompson et al., 2012). In brief, a candidate DNA promoter element was cloned into
571 the pCCT expression vector between an arabinose-inducible pBAD promoter and the
572 reporter gene *lacZ*. This plasmid was co-transformed into BL21 (DE3) *E. coli* along with
573 an IPTG-inducible pET151 expression vector with (pET151-YtgR) or without (pET151-
574 EV) the C-terminal 139 amino acid residues of CTL0325 (YtgC). Note that we have
575 previously demonstrated that this region is a functional iron-dependent repressor

576 domain (Thompson et al., 2012). To verify the functionality of this assay, we determined
577 whether ectopic YtgR expression could repress pCCT reporter gene expression in the
578 presence of three candidate DNA elements: a no-insert empty vector (pCCT-EV), the
579 putative promoter element for *C. trachomatis lpdA* (pCCT-*lpdA*), and the promoter
580 region of the *ytgABCD* operon (pCCT-*ytgABCD*; Figure 5B). As expected, from the
581 pCCT-EV reporter construct, ectopic YtgR expression did not significantly reduce the
582 activity of β-galactosidase. Additionally, reporter gene expression from pCCT-*lpdA*,
583 containing the promoter of iron-regulated *lpdA* (Brinkworth et al., 2018), which is not
584 known to be YtgR-regulated, was not affected by ectopic expression of YtgR. This
585 demonstrated that the assay can discriminate between the promoter elements of iron-
586 regulated genes and *bona fide* YtgR targeted promoters. Indeed, in the presence of
587 pCCT-*ytgABCD*, induction of YtgR expression produced a significant decrease in β-
588 galactosidase activity (p = 0.03868) consistent with its previously reported auto-
589 regulation of this promoter (Thompson et al., 2012).
590 Using this same assay, we then inserted into the pCCT reporter plasmid 1) the
591 *trpR* promoter element (pCCT-*trpR*), 2) the putative *trpBA* promoter element
592 represented by the IGR (pCCT-*trpBA*), and 3) the same putative *trpBA* promoter
593 element with a mutated YtgR operator sequence that was diminished for both
594 palindromicity and A-T richness, two typical features of prokaryotic promoter elements
595 (pCCT-*trpBA*ΔOperator; Figure 5C) (Schmitt, 2002; Tao, Boydt, & Murphy, 1992). When
596 YtgR was ectopically expressed in the pCCT-*trpR* background, we observed no
597 statistically distinguishable change in β-galactosidase activity. However, in the pCCT-
598 *trpBA* background, ectopic YtgR expression significantly reduced β-galactosidase

599 activity at levels similar to those observed in the pCCT-*ytgABCD* background (*p* =
600 0.01219). This suggested that YtgR was capable of binding to the *trpBA* promoter
601 element specifically. Interestingly, this repression phenotype was abrogated in the
602 pCCT-*trpBA*ΔOperator background, where we observed no statistically meaningful
603 difference in β-galactosidase activity. We subsequently addressed whether the region of
604 the *trpRBA* IGR containing the YtgR operator site was sufficient to confer YtgR
605 repression in this assay (Figure 5 – Figure Supplement 1). We cloned three fragments
606 of the *trpRBA* IGR into the pCCT reporter plasmid: the first fragment represented the 5'-
607 end of the IGR containing the operator site at the 3'-end (pCCT-IGR1), the second
608 fragment represented a central region of the IGR containing the operator site at the 5'-
609 end (pCCT-IGR2), and the third fragment represented the 3'-end of the IGR and did not
610 contain the operator site (pCCT-IGR3). Surprisingly, we observed that none of these
611 fragments alone were capable of producing a significant repression phenotype in our
612 reporter system. This finding indicated that while the operator site was necessary for
613 YtgR repression, it alone was not sufficient. Together, these data indicated that YtgR
614 could bind to the *trpBA* promoter element and that this binding was dependent upon an
615 intact AT-rich palindromic sequence, likely representing an YtgR operator, but that
616 further structural elements in the *trpRBA* IGR may be necessary for repression.
617 Nonetheless, we demonstrated the existence of a functional YtgR binding site that
618 conferred iron-dependent transcriptional regulation to *trpBA*, independent of the major
619 *trpR* promoter.
620
621

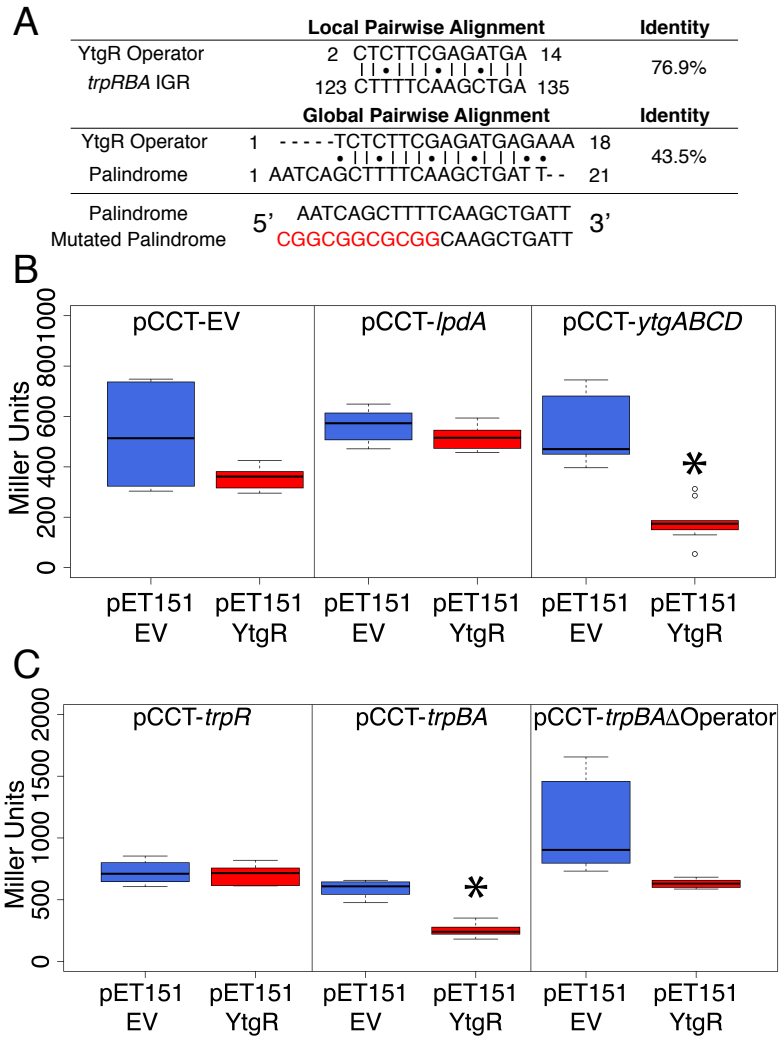

Figure 5. Ectopically expressed YtgR domain is capable of binding the putative *trpBA* promoter element in an operator-specific manner to repress transcription in a heterologous system. (*A*) Identification of putative YtgR operator sequence by local and global nucleotide sequence alignment using EMBOSS Water and Needle algorithms, respectively, to align the previously identified YtgR operator to both the *trpRBA* IGR and palindromic candidate sequence. The palindrome was then mutated in our YtgR repression assay as depicted to abolish palindromicity and AT-richness. (*B*) Ectopic expression of YtgR significantly represses β-galactosidase activity only from the promoter of its own operon, *ytgABCD*, and not from an empty vector or another iron-regulated but presumably non-YtgR targeted promoter, *lpdA.* N = 2 or 3. (*C*) Expression of recombinant YtgR represses β-galactosidase activity from the putative *trpBA* promoter element, but not the *trpR* promoter, and this repression is dependent on the unaltered operator sequence identified in Fig. 5A. N = 2 or 3. Statistical significance determined by two-sided unpaired Student's *t*-test with Welch's correction for unequal variance. * = $p < 0.05$, ** = $p < 0.01$, *** = $p < 0.005$.

652 **Transcripts initiated at the primary *trpR* promoter terminate at the YtgR operator**
653 **site.** We hypothesized that YtgR binding at the *trpRBA* YtgR operator site may
654 disadvantage the processivity of RNAP reading-through the IGR from the upstream *trpR*
655 promoter. Similar systems of RNAP read-through blockage have been reported; the
656 transcription factor Reb1p "roadblocks" RNAPII transcription read-through in yeast by
657 promoting RNAP pausing and subsequent degradation (Colin et al., 2014). To
658 investigate this question, we first returned to RNA-Sequencing data we generated to
659 define the immediate iron-dependent transcriptional regulon in *C. trachomatis*
660 (Brinkworth et al., 2018). Using data obtained from *C. trachomatis*-infected HeLa cells at
661 12 hpi + 6h mock or Bpdl treatment, we mapped the sequenced reads in batch across
662 three biological replicates to the *C. trachomatis* L2 434/Bu genome (NC_010287) which
663 we modified to include annotations for non-operonic IGRs. This coverage map indicated
664 that under Bpdl-treated conditions, a higher proportion of reads mapped to the *trpRBA*
665 IGR (IGR_trpB) relative to mock-treatment (Figure 6A). However, a notable increase in
666 reads mapping to the upstream *trpR* CDS was not observed, suggesting that under iron
667 replete conditions, transcripts originating from the primary *trpR* promoter may be
668 terminated before reading through the IGR. Note that this is consistent with the original
669 observation that *trpR* is not differentially expressed under iron-limited conditions in this
670 RNA-Seq dataset (Brinkworth et al., 2018). We additionally investigated the abundance
671 of reads mapping to the IGRs upstream of *euo* (IGR_euo; not iron-regulated, not YtgR-
672 regulated) and *lpdA* (IGR_lpdA; iron-regulated, not YtgR-regulated), and were unable to
673 observe a similar increase in read coverage at these IGRs following Bpdl treatment,
674 indicating that the increased coverage at the *trpRBA* IGR was specific (Figure 6 –

675 Figure Supplement 1A-B). The absolute number of reads mapping to the *trpRBA* IGR
676 under these conditions was very low relative to either upstream or downstream CDS,
677 implying that the terminated transcript species are rare. We therefore turned to more
678 sensitive and quantitative methods to interrogate possible transcript termination within
679 the *trpRBA* IGR.

680 To identify transcription termination sites (TTSs) in the *trpRBA* operon in *C.*
681 *trachomatis*, we utilized 3'-RACE to map the 3'-ends of transcripts using gene-specific
682 primers within the *trpR* CDS (Figure 6B; bottom). We again utilized two RACE
683 amplification cycles to generate distinct, specific bands suitable for isolation and
684 sequencing (Figure 6 – Figure Supplement 2B-C). By gel electrophoresis of the 3'-
685 RACE products, we observed the appearance of four distinct bands that migrated with
686 an apparent size of 0.55, 0.45, 0.40 and 0.20 kb. In our Trp-depleted condition, we
687 observed only a very weak amplification of the 2.5 – 3 kb full-length *trpRBA* message by
688 3'-RACE (Figure 6 – Figure Supplement 2A). However, we did observe it across all
689 replicates. To confirm that the full-length product was specific to the Trp-deplete
690 treatment, we amplified the *trpRBA* operon by RT-PCR from the 3'-RACE total RNA
691 (Figure 6B; top). As expected, only in the Trp-deplete sample did we observe robust
692 amplification of the full-length *trpRBA* message. We note however that image contrast
693 adjustment reveals a very weak band present in all experimental samples. In
694 accordance with the RNA-Sequencing data, 3'-RACE demonstrated the presence of
695 unique transcription termination events in the *trpRBA* operon.

696 To identify the specific TTS locations, we gel extracted the four distinct 3'-RACE
697 bands across all conditions and cloned them into the pRACE sequencing vector as was

698 done for the 5'-RACE experiments. We then sequenced the inserted RACE products
699 and mapped them to the *C. trachomatis* L2 434/Bu genome (Figure 6B). This revealed a
700 highly dynamic TTS landscape within the *trpRBA* IGR, which has not previously been
701 investigated (For a full description of mapped 3'-RACE products, see Supplementary
702 File 2). The 0.20 kb RACE product mapped to the 3'-end of the *trpR* CDS, with a mean
703 nucleotide position of 511,665 and a modal nucleotide position of 511,667 (Figure 6 –
704 Figure Supplement 3A). Contrastingly, the other three 3'-RACE products did not map in
705 such a way so as to produce specific, unambiguous modal peaks. Instead, their
706 distribution was broader and more even, with only a few nucleotide positions mapping
707 more than once. Accordingly, the 0.45 kb product mapped with an average nucleotide
708 position of 511,889, just downstream of the 1.1 kb 5'-RACE product (Figure 6 – Figure
709 Supplement 3C), while the 0.55 kb product mapped with an average nucleotide position
710 of 511,986, upstream of the 1.0 kb 5'-RACE product (Figure 6 – Figure Supplement
711 3D). Interestingly, the 0.40 kb product mapped to a region directly overlapping the
712 putative YtgR operator site, with a mean nucleotide position of 511,811 (Figure 6 –
713 Figure Supplement 3B). We therefore reasoned that this putative TTS may have an
714 iron-dependent function.
715
716
717
718
719
720

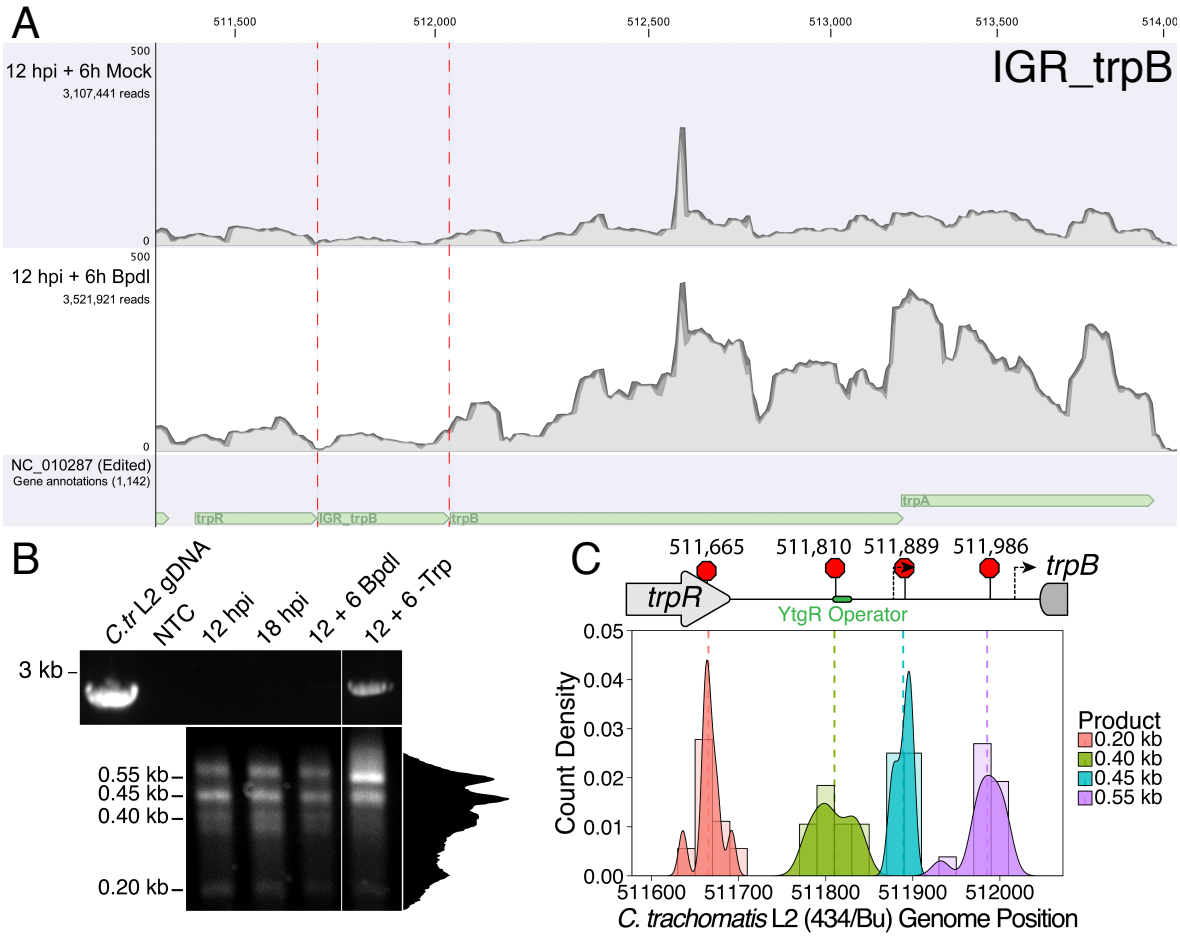

Figure 6. Transcription from the primary *trpR* promoter terminates in the *trpRBA* IGR region, notably at the YtgR operator site. (*A*) Coverage map of RNA-Sequencing reads mapped to the *C. trachomatis* L2/434 Bu genome (NC_010287) edited to contain annotations for non-operonic IGRs. Read coverage at the *trpRBA* IGR (IGR_trpB) is increased following Bpdl treatment, but *trpR* read coverage is not similarly increased. (*B*) Total RNA was harvested from *C. trachomatis*-infected HeLa cells to analyze 3'-cDNA landscape downstream of the *trpR* promoter. The top panel displays representative RT-PCR of full-length *trpRBA* message across experimental conditions (NTC = No Template Control). Bottom panel depicts electrophoresed 3'-RACE products and estimated sizes. Intensity plot to the right of image was generated using the Fiji Dynamic ROI Profiler plugin to monitor intensity across the 18 hpi condition. Note the presence of four distinct peaks, corresponding to each 3'-RACE product. N=3. (*C*) 3'-RACE products were sequenced and mapped to *C. trachomatis* L2 434/Bu genome by nucleotide BLAST. Figure displays histogram (semi-continuous; bin width=20) and overlaid density plot (continuous) distribution of 3' nucleotide positions generated from each 3'-RACE product. The dotted line represents the weighted mean of the distribution, as indicated by the integer value above each line. The identified alt. TTSs are depicted on the *trpRBA* operon (drawn to scale) above the plot. The 0.40 kb RACE product mapped to a region overlapping the predicted YtgR operator site. N=3.

754 **Iron limitation promotes transcription read-through at the YtgR operator site.**
755 Given the observation that transcripts terminated at the YtgR operator site, we
756 hypothesized that YtgR binding may promote transcription termination at this locus.
757 Conversely, we hypothesized that inactivating YtgR DNA-binding by Bpdl treatment
758 would allow transcription to read through the YtgR operator site. To quantitatively
759 analyze the possibility that iron-depletion, and thus dissociation of YtgR, may facilitate
760 transcription read-through at the operator site, we utilized RT-qPCR to monitor the
761 abundance of various amplicons across the *trpRBA* operon (Figure 7A). We quantified
762 these data in relation to a "read-through" normalization amplicon that, based on 5'- and
763 3'-RACE data, should only be represented when the full-length *trpRBA* message is
764 transcribed (Figure 7A). The representation of a specific mRNA species relative to the
765 full-length transcript should therefore be interpretable through a simple ratio of the
766 experimental amplicon to the "read-through" amplicon. If an mRNA species is poorly
767 represented relative to the full-length transcript, the ratio should be approximately 1.0.
768 Conversely, if that species is over-represented relative to the full-length transcript, the
769 ratio should exceed 1.0 (Figure 7B; left). Therefore, as each amplicon is increasingly
770 represented as a part of the full-length transcript, the ratio of the specific amplicon to the
771 normalization amplicon should approach 1.0 (Figure 7B; right).
772 We first analyzed an amplicon from nucleotide 511,416 – 531 to monitor the
773 relative abundance of transcript species associated with transcription initiating at the
774 *trpR* promoter (Figure 7C). We observed that the representation of this amplicon was
775 not significantly altered following iron limitation relative to 12 hpi, suggesting that the
776 depletion of iron was not affecting initiation of transcription at the *trpR* promoter.

777 Interestingly, at 18 hpi, the representation ratio of this amplicon significantly shifted
778 further away from 1.0 (p = 0.00358), indicating that at 18 hpi this amplicon is
779 represented less as a component of read-through transcription relative to 12 hpi. As
780 expected, under Trp-deplete conditions, the representation ratio shifted significantly
781 closer to 1.0 (p = 0.00064), consistent with read-through transcription of the full-length
782 *trpRBA* message.

783 We then preformed the same analysis on an amplicon from nucleotide 511,639 –
784 764, immediately upstream of the TTS at the YtgR operator site to monitor condition-
785 dependent read-through at this site (Figure 7D). We again observed that at 18 hpi, the
786 representation ratio was significantly increased (p = 0.01046), and following Trp-
787 depletion, the ratio was significantly decreased (p = 0.00023), as expected. Notably,
788 and consistent with our hypothesis, we observed that the representation ratio of this
789 amplicon was also significantly closer to 1.0 following iron limitation (p = 0.00407),
790 suggesting that transcription read-through was increased at this site under iron limited
791 conditions. Indeed, if YtgR is dissociating from the operator site during iron depletion, a
792 greater proportion of transcripts would be expected to read-through this locus.

793 Finally, we analyzed an amplicon from nucleotide 513,856 – 968, at the very 3'-
794 end of *trpA* to asses changes in terminal transcription under our experimental conditions
795 (Figure 7E). At 18 hpi, we observed a significant increase in the representation ratio of
796 this amplicon (p = 0.00476), which is likely attributable to both basal levels of alternative
797 transcription from the IGR as well as poor transcription read-through of the full-length
798 message. Following 6 hrs of Bpdl treatment, we also observed a significant increase in
799 the representation ratio of this amplicon (p = 0.01510), which supports the finding that

800 *trpBA* is being preferentially transcribed under this condition, distinct from the full-length
801 *trpRBA* transcript. We were only able to detect a marginal decrease in the
802 representation of this amplicon under Trp-depleted conditions (p = 0.07942), which may
803 suggest that the very 3'-end of *trpRBA* is under-represented relative to our
804 normalization amplicon, which falls within the middle of the operon. In fact, recent work
805 has reported on the relatively poor representation of 3'-end mRNAs in *Chlamydia*
806 (Ouellette, Rueden, & Rucks, 2016). In sum, this set of experiments provides evidence
807 that iron-depletion specifically alters the representation of particular mRNA species
808 across the *trpRBA* operon. Additionally, they implicate iron-dependent YtgR DNA-
809 binding as the mediator of these effects. By alleviating YtgR repression via iron
810 depletion, transcription is allowed to proceed through the operator site, albeit at basal
811 levels. Concomitantly, transcription is specifically activated at the downstream alt. TSS
812 for *trpBA*.
813
814
815
816
817
818
819
820
821
822

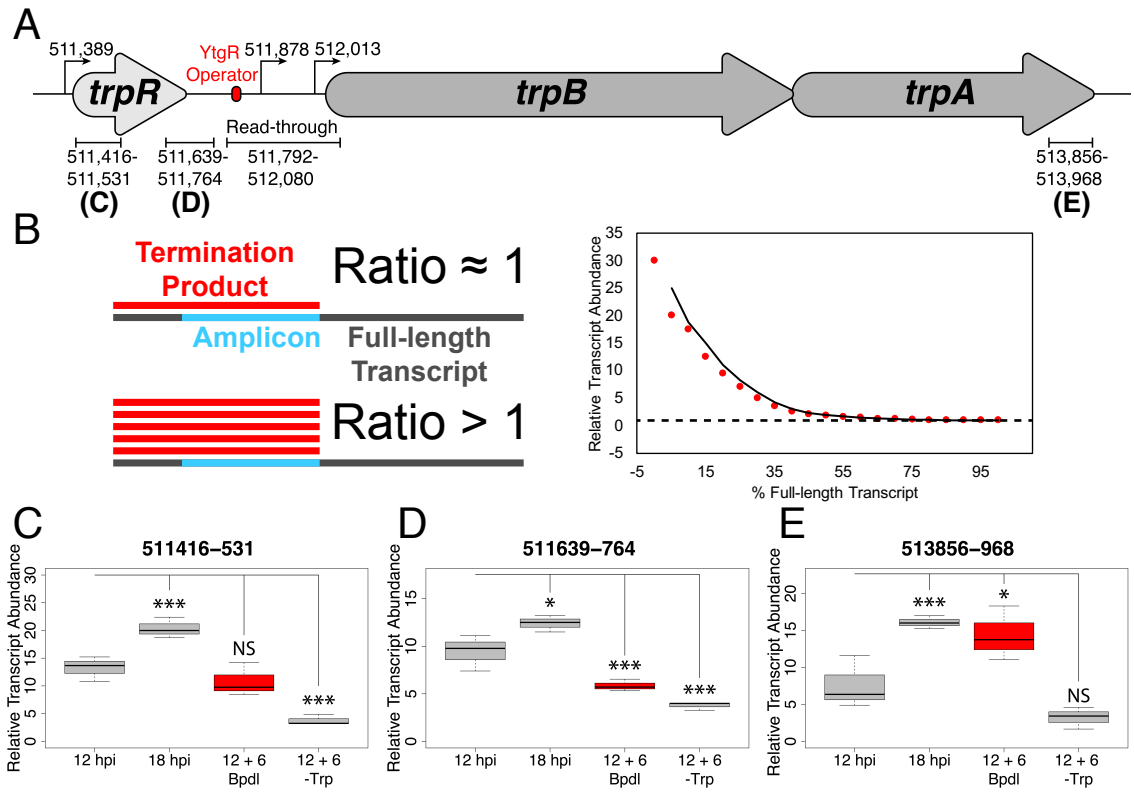

Figure 7. Iron limitation promotes transcription read-through at the YtgR operator site. (*A*) Cartoon depiction of amplicons analyzed in these experiments across the *trpRBA* operon, with the identified TSSs and YtgR operator site anootated. Drawn to scale. (*B*) Schematic representation of RT-qPCR analysis. On the left, a biological interpretation of the ratio used to determine the relative transcript abundance is provided. When a termination product (red) is poorly represented, *e.g.* read-through is high, the ratio of specific amplicon (blue) to full-length transcript (grey) should be close to 1.0. When the termination product is abundant, *e.g.* read-through is low, then the ratio should exceed 1.0. On the right, a graphical demonstration of this concept is provided using mock data. The dotted line represents the theoretical asymptote at a value of 1.0. (*C*) Analysis of transcription read-through by RT-qPCR was performed on 3'-RACE total RNA at three distinct loci across the *trpRBA* operon representing upstream transcription initiation (511,416-531), (*D*) YtgR operator site termination (511,639-764) and (*E*) terminal *trpBA* transcription (513,856-968). Abundance of each amplicon was normalized to a region (Read-through) predicted to be transcribed only as a part of the full-length product based on 5' and 3'-RACE data (511,792-512,080). Thus, the ratio of each amplicon to the normalization amplicon represents the proportion of that amplicon encoded as part of the full-length transcript. At the YtgR operator termination site, iron limitation reduces the ratio relative to 12 hpi, suggesting that transcription read-through increases at this site under this condition. Statistical significance determined by One-way ANOVA followed by post-hoc pairwise *t*-tests. * = $p < 0.05$, ** = $p < 0.01$, *** = $p < 0.005$.

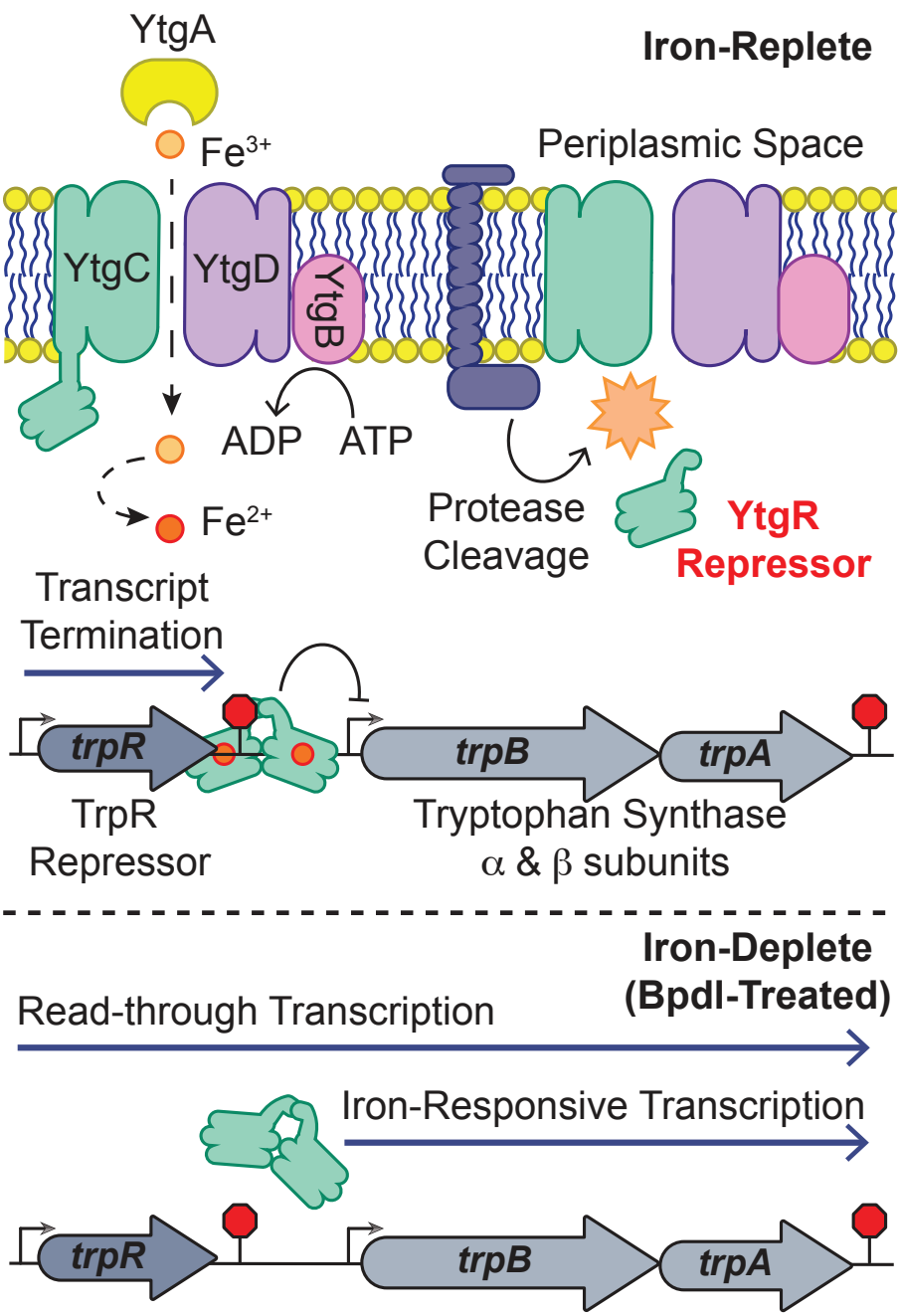

Figure 8. Model for proposed mechanism of iron-dependent YtgR-mediated regulation of *trpRBA* expression. Iron is imported through the YtgABCD ABC-type metal permease complex. YtgR is cleaved from the YtgCR permease-repressor fusion protein. In the presence of sufficient iron, holo-YtgR can bind to the *trpRBA* IGR to both terminate basal transcription from the primary *trpR* promoter and repress transcription initiation at the alternative *trpBA* promoter. Iron depletion inactivates YtgR DNA-binding, thus promoting read-through of basal transcription from the *trpR* promoter while also inducing transcription at the downstream *trpBA* promoter.

884 **Discussion**

885 In this study, we provide a mechanistic explanation for the specific iron-limited
886 induction of *trpBA* expression mediated by the repressor YtgR, representing a novel
887 instance of integrated stress adaptation in *Chlamydia*. Utilizing an infected-epithelial cell
888 culture model, we identified a previously undescribed iron-regulated promoter element
889 within the *trpRBA* IGR responsible for the iron-limited induction of *trpBA* expression
890 independent of *trpR.* Using *in silico*, biochemical and chemical-genetic methods, we
891 demonstrate that YtgR binds the *trpRBA* IGR to regulate iron-dependent *trpBA*
892 expression. Importantly, transcriptional repression in our heterologous system was
893 shown to be dependent on an unaltered operator sequence that bears significant
894 homology to the previously defined operator element in the *ytg* promoter. Previously
895 published reports have demonstrated that YtgR is capable of directly binding DNA
896 sequences containing this operator *in vitro* (Akers et al., 2011; Thompson et al., 2012).
897 Furthermore, our infected-cell culture studies revealed that transcripts originating from
898 the primary *trpR* promoter terminate within the IGR, notably at the putative YtgR
899 operator site, and that transcription read-through at this locus is iron-dependent. Thus,
900 we propose that YtgR regulates *trpBA* expression at two levels: repression of the *trpBA*
901 promoter and premature termination of the major transcript generated from the *trpR*
902 promoter (Figure 8). This is the first time an iron-dependent mode of regulation has
903 been shown to control the expression of tryptophan biosynthesis in prokaryotes, which
904 reflects the uniquely specialized nature of *C. trachomatis*.

905 While we demonstrate here that iron-dependent *trpBA* expression originates from
906 a novel promoter element immediately upstream of the *trpB* CDS, this is not the first

907 description of an alt. TSS within the *trpRBA* IGR. Carlson, *et al*. identified an alt. TSS
908 within the IGR which they suggested was responsible for *trpBA* expression (Carlson et
909 al., 2006). In these studies, we were unable to confirm the presence of the previously
910 identified alt. TSS by 5'-RACE. This is likely because Carlson, *et al*. examined the
911 presence of transcript origins following 24 hrs of Trp starvation whereas here we
912 monitored immediate responses to stress following only 6 hrs of treatment. Prolonged
913 Trp depletion would result in a more homogeneously stressed population of chlamydial
914 organisms that may exhibit the same preferential utilization of the promoter identified by
915 Carlson, *et al*., the detection of which is precluded in a more heterogeneous, transiently-
916 stressed population. This may explain the observation of multiple T(S/T)Ss across the
917 *trpRBA* operon in our studies. However, the contribution of such a Trp-dependent alt.
918 TSS as identified by Carlson *et al.* to the general stress response of *C. trachomatis*
919 remains unclear given its association with presumably abnormal organisms. Does
920 utilization of this alt. TSS indicate abnormal growth or a *bona fide* stress adaptation?
921 Moreover, Akers & Tan were unable to verify TrpR binding to the *trpRBA* IGR by EMSA,
922 suggesting that some other Trp-dependent mechanism may control transcription from
923 this site (Akers & Tan, 2006). Ultimately, our approach of investigating more immediate
924 responses to stress revealed previously unreported mechanisms functioning to regulate
925 Trp biosynthesis in *C. trachomatis*, underscoring the value of transient as opposed to
926 sustained induction of stress.
927 Another mechanism of regulation reported to control the chlamydial *trpRBA*
928 operon is Trp-dependent transcription attenuation. Based on sequence analysis, a
929 leader peptide has been annotated within the *trpRBA* IGR (Merino & Yanofsky, 2005).

930 Presumably, this functions analogously to the attenuator in the *E. coli trpEDCBA*
931 operon; Trp starvation causes ribosome stalling at sites of enriched Trp codons such
932 that specific RNA secondary structures form to facilitate RNAP read-thru of downstream
933 sequences – in this case, *trpBA* (Yanofsky, 1981). However, robust experimental
934 evidence to support the existence of attenuation in *C. trachomatis* is lacking. To date,
935 the only experimental evidence that supports this model was reported by Carlson, *et al*.,
936 who demonstrated that in a TrpR-mutant genetic background, an additional increase in
937 *trpBA* expression could be observed following 24 hr Trp-depletion. (Carlson et al.,
938 2006). However, this could be attributable to an alternative Trp-dependent, *but TrpR-*
939 *independent* mechanism controlling *trpBA* expression at the alt. TSS identified by
940 Carlson, *et al*. None of the data presented here point conclusively to the existence of a
941 Trp-dependent attenuator. The additional termination sites identified in our 3'-RACE
942 assay may represent termination events mediated by an attenuator, but without more
943 specific analysis utilizing mutated sequences we cannot attribute attenuator function to
944 those termination sites.

945 Interestingly, in *Bacillus subtilis,* Trp-dependent attenuation of transcription takes
946 on a form markedly different from that in *E. coli*. Whereas attenuation functions in *cis* for
947 the *E. coli trp* operon, *B. subtilis* utilize a multimeric Tryptophan-activated RNA-binding
948 Attenuation Protein, TRAP, which functions in *trans* to bind *trp* operon RNA under Trp-
949 replete conditions, promoting transcription termination and inhibiting translation
950 (Gollnick, Babitzke, Antson, & Yanofsky, 2005). This interaction is antagonized by anti-
951 TRAP in the absence of charged $tRNA^{Trp}$, leading to increased expression of TRAP
952 regulated genes. We suggest that YtgR may represent the first instance of a separate

953 and distinct clade of attenuation mechanisms: iron-dependent *trans*-attenuation. This
954 mechanism may function independently of specific RNA secondary structure, relying
955 instead on steric blockage of RNAP processivity, but ultimately producing a similar
956 result. Possible regulation of translation remains to be explored. The recent
957 development of new genetic tools to alter chromosomal sequences and generate
958 conditional knockouts in *C. trachomatis* should enable a more detailed analysis of
959 *trpRBA* regulation, including possible *trans*-attenuation (Mueller, Wolf, & Fields, 2016;
960 Ouellette, 2018).

961 As a Trp auxotroph, what might be the biological significance of iron-dependent
962 YtgR regulation of the *trpRBA* operon in *C. trachomatis*? We have already noted the
963 possibility that iron-dependent *trpBA* regulation in *C. trachomatis* may enable the
964 induction of a similar response to both Trp and iron starvation, stimuli likely mediated by
965 IFN-γ *in vivo*. This mechanism also presents the opportunity for *C. trachomatis* to
966 respond similarly to distinct *sequential* stresses, where a particular stress may prime the
967 pathogen to better cope with subsequent stresses. To reach the female upper genital
968 tract (UGT), where most significant pathology is identified following infection with *C.*
969 *trachomatis*, the pathogen must first navigate the lower genital tract (LGT). *Chlamydia*
970 infections of the female LGT are associated with bacterial vaginosis (BV), which is
971 characterized by obligate and facultative anaerobe colonization, some of which produce
972 indole (Sasaki-Imamura, Yoshida, Suwabe, Yoshimura, & Kato, 2011; Ziklo, Huston,
973 Hocking, & Timms, 2016). This provides *C. trachomatis* with the necessary substrate to
974 salvage tryptophan via TrpBA. Interestingly, the LGT is also likely an iron-limited
975 environment. Pathogen colonization and BV both increase the concentration of mucosal

976 lactoferrin (Lf), an iron-binding glycoprotein, which can starve pathogens for iron (Spear
977 et al., 2011; Valenti et al., 2018). Lf expression is additionally hormone-regulated, and
978 thus the LGT may normally experience periods of iron limitation (Cohen, Britigan,
979 French, & Bean, 1987; Kelver et al., 1996). Moreover, the expression of TfR is
980 constrained to the basal cells of the LGT stratified squamous epithelium (Lloyd,
981 O'Dowd, Driver, & Tee, 1984), which likely restricts necessary Tf-bound iron from *C.*
982 *trachomatis* infecting the accessible upper layers of the stratified epithelia (Nogueira,
983 Braun, & Carabeo, 2017; Ouellette & Carabeo, 2010).
984 For *C. trachomatis*, iron limitation may therefore serve as a critical signal in the
985 LGT, inducing the expression of *trpBA* such that Trp is stockpiled from available indole,
986 allowing the pathogen to counteract impending IFN-γ-mediated Trp starvation. We
987 suggest the possibility that iron limitation in the LGT may be a significant predictor of
988 successful pathogen colonization in the UGT. Unfortunately, testing these hypotheses in
989 cell culture models of infection presents a significant challenge. Evaluating rescue of
990 chlamydial growth in the presence of indole to specifically assess the iron-dependent
991 role of *trpBA* requires simultaneous Trp and iron depletion. The former ensures indole
992 utilization by the bacteria, and the latter de-represses YtgR-regulated *trpBA* expression.
993 In theory, this is feasible, but in practice the combined stress rapidly induces aberrant
994 development, muddying results obtained from such studies (data not shown). Ideally,
995 genetic approaches could be employed to distinguish the regulatory effects of YtgR
996 independent of TrpR. However, the genetic manipulation of *trans*-acting factors (*e.g.*
997 YtgR) will presumably have unpredictable off-target effects. Genetically altering *cis*-
998 acting factors – such as operator sequences – is more feasible, but at present we lack

999 the information necessary to rationally mutate these sequences in *C. trachomatis* to
1000 interrogate these questions. The tight regulatory coordination at both the transcription
1001 initiation and termination steps would likely mean any mutation in the *cis*-acting
1002 sequences would affect both processes indiscriminately. Furthermore, *in vivo* infection
1003 models present challenges: attempting to answer these questions will likely require the
1004 use of *in vivo* non-human primate studies, as mouse models of *Chlamydia*-infection do
1005 not recapitulate immune-mediated Trp starvation (Nelson et al., 2005). Ultimately, these
1006 limitations do not undermine the biological significance of an iron-dependent mode of
1007 regulating Trp salvage, given the critical role played by this pathway during infection.
1008 Finally, and of note, the expression of the ribonucleotide diphosphate-reductase-
1009 encoding *nrdAB* was also recently shown to be iron-regulated in *C. trachomatis*
1010 (Brinkworth et al., 2018). The regulation of *nrdAB* is known to be mediated by the
1011 presumably deoxyribonucleotide-dependent transcriptional repressor NrdR, encoded
1012 distal to the *nrdAB* locus (Case, Akers, & Tan, 2011). As NrdR activity is not known to
1013 be modulated by iron availability, this raises the intriguing possibility that here too a
1014 unique iron-dependent mechanism of regulation may integrate the chlamydial stress
1015 response to promote a unified response across various stress conditions. Future studies
1016 may require more metabolomics-based approaches to thoroughly dissect the integration
1017 of these stress responses, as transcriptome analyses alone often miss broader,
1018 pathway-oriented metabolic coordination. Ultimately, these studies point towards a need
1019 to carefully re-evaluate the molecular stress response in *Chlamydia*, with greater
1020 emphasis on the use of targeted approaches and treatment protocols that induce stress,
1021 but not persistence. We anticipate that the rapid progress of the field in recent years will

1022 continue to catalyze exciting and important discoveries regarding the fundamental

1023 biology of *Chlamydia*.

1024 **Materials and Methods**

1025 **Eukaryotic Cell Culture and Chlamydial Infections**
1026 Human cervical epithelial adenocarcinoma HeLa (ATCC® CCL-2) cells were cultured at
1027 37° C with 5% atmospheric CO_2 in Dulbecco's Modified Eagle Medium (DMEM)
1028 supplemented with 10 μg/mL gentamicin, 2 mM L-glutamine, and 10% (*v/v*) filter
1029 sterilized fetal bovine serum (FBS). For all experiments, HeLa cells were cultured
1030 between passage numbers 4 and 16. *Chlamydia trachomatis* serovar L2 (434/Bu) was
1031 originally obtained from Dr. Ted Hackstadt (Rocky Mountain National Laboratory,
1032 NIAID). Chlamydial EBs were isolated from infected HeLa cells at 36-40 hours post-
1033 infection (hpi) and purified by density gradient centrifugation essentially as described
1034 (Caldwell, Kromhout, & Schachter, 1981).
1035
1036 For the infection of 6-well tissue culture plates, HeLa cells cultured to 80-90%
1037 confluency were first washed with pre-warmed Hanks Buffered Saline Solution (HBSS)
1038 prior to the monolayer being overlaid with inoculum (un-supplemented DMEM) at the
1039 indicated multiplicity of infection (MOI). Tissue culture plates were then centrifuged at 4°
1040 C with a speed of 1000 RPM (Eppendorf 5810 R table top centrifuge, A-4-81 rotor) for 5
1041 minutes to synchronize the infection. Inoculum was aspirated and cells were washed
1042 again with pre-warmed HBSS prior to the media being replaced with pre-warmed
1043 complete DMEM. Infected cultures were then returned to the tissue culture incubator
1044 until the indicated times post-infection. This procedure was replicated exactly for the
1045 infection of 24-well tissue culture plates.
1046
1047 **Iron Starvation**
1048 *Chlamydia trachomatis* L2-infected HeLa cell cultures were starved for iron by
1049 supplementation of the media with the iron chelator 2,2-bipyridyl (Bpdl; Sigma Aldrich,
1050 St. Louis, MO, USA; CAS: 366-18-7) essentially as described (Thompson & Carabeo,
1051 2011). Briefly, at the indicated times post-infection, infected cell cultures were washed
1052 with pre-warmed HBSS prior to the addition of complete DMEM (mock) or complete
1053 DMEM supplemented with 100 μM Bpdl. Infected cell cultures were returned to the
1054 incubator for the indicated treatment periods. Bpdl was prepared as a 100 mM stock
1055 solution in 100% ethanol and stored at -20° C for no longer than 6 months.
1056
1057 **Tryptophan Starvation**
1058 *Chlamydia trachomatis* L2-infected HeLa cell cultures were starved for tryptophan by
1059 replacement of complete DMEM with tryptophan-depleted medium. In brief, Tryptophan-
1060 replete or –deplete DMEM-F12 (U.S. Biological Life Sciences, Salem, MA, USA)
1061 powder media was prepared following manufacture instructions and supplemented with
1062 10% (*v/v*) filter-sterilized FBS which had been previously dialyzed 16-20h at 4° C in PBS
1063 in a 10 kDa MWCO dialysis cassette. Media was then further supplemented with 10
1064 μg/mL gentamicin. At the indicated times post-infection, complete DMEM was aspirated

1065 and wells were washed with pre-warmed HBSS prior to the addition of tryptophan-
1066 replete or –deplete medium. Infected cell cultures were returned to the incubator for the
1067 indicated treatment periods.
1068
1069 **Cloning**
1070 All constructs were cloned using standard molecular cloning techniques, *e.g.* restriction
1071 enzyme, homology-directed, etc. All primers and plasmids used in this study can be
1072 found in Supplementary file 3 and 4, respectively.
1073
1074 **Immunofluorescent Confocal Microscopy**
1075 At the indicated times post-infection, *C. trachomatis* L2-infected HeLa cell cultures
1076 seeded on glass coverslips in 24-well tissue cultures plates were first washed with pre-
1077 warmed HBSS prior to fixation with 4% paraformaldehyde (PFA) in phosphate buffered
1078 saline (PBS) for 20 minutes at RT ° C. Fixation solution was aspirated and wells were
1079 washed with PBS prior to permeabilization with 0.2% Triton X-100 in PBS for 5 minutes
1080 at RT° C. Permeabilization solution was then decanted and cells were washed with
1081 PBS. The coverslips were blocked for 30 minutes with 1% bovine serum albumin (BSA)
1082 in PBS at RT° C. To stain for *Chlamydia*, coverslips were washed with PBS and PBS
1083 supplemented with 1% BSA and 1:500 convalescent human sera was added to wells
1084 and incubated at RT° C for 1 hour with rocking. Primary antibody solution was decanted
1085 and coverslips were again washed with PBS. Goat anti-human Alexa-647 (Invitrogen,
1086 ThermoFisher Scientific, Waltham, MA, USA) diluted 1:1000 in PBS with 1% BSA was
1087 then added to the wells and incubated in the dark for another hour at RT° C with
1088 rocking. Secondary antibody solution was then decanted, coverslips were washed again
1089 with PBS and coverslips were either immediately mounted on microscopy slides using
1090 ImmuMount (ThermoFisher Scientific) or VectaShield H-1000 (Vector Laboratories,
1091 Burlingame, CA, USA) or stored in the dark at 4° C until mounting. All images were
1092 acquired on a Leica TCS SP8 laser scanning confocal microscope, using identical
1093 settings, in the Integrative Physiology and Neuroscience Advanced Imaging Center at
1094 Washington State University. All images are Z-projections and were processed in Fiji
1095 (Schindelin et al., 2012) and Adobe Creative Suite identically for each comparative time-
1096 point.
1097
1098 **Nucleic Acid Preparation**
1099 RNA was harvested from *C. trachomatis*-infected HeLa cell monolayers by scraping 3
1100 wells of a 6-well plate in ice-cold Trizol® Reagent (ThermoFisher Scientific). Samples
1101 were then pooled and split into two technical replicates (RT-qPCR) or kept as one
1102 biological replicate (RACE). Trizol®-extracted samples were then thoroughly vortexed
1103 with a 100 μL volume of Zirconia beads prior to chloroform extraction. 100% ethanol
1104 was added to the aqueous phase and RNA was isolated using the Ambion®
1105 RiboPure™ RNA Purification kit for bacteria following manufacturer instructions
1106 (ThermoFisher Scientific). DNA was removed from RNA samples using the Invitrogen
1107 DNA-*free*™ DNA Removal Kit following manufacturer instructions (ThermoFisher
1108 Scientific). RNA was stored at -20° C until further use.
1109

1110 cDNA was generated using either SuperScript® IV Reverse Transcriptase (RT-qPCR;
1111 ThermoFisher Scientific) or SMARTScribe™ Reverse Transcriptase (RACE and RACE-
1112 specific qRT-PCR); Takara Bio, Kusatsu, Shiga Prefecture, Japan) essentially as
1113 described by the respective manufacturers. For cDNA generated for RT-qPCR, 650 ng
1114 of total RNA was used as a template in a 20 μL total reaction volume. For every RT
1115 reaction, a "no-RT" control, generated from 350 ng of total RNA template in a 10 μL total
1116 volume, was included. For 5'-RACE, cDNA was generated from 250 ng of total RNA
1117 using random primers in a 10 μL total volume and further processed in the RACE
1118 workflow. cDNA was stored at -20° C.
1119
1120 gDNA was harvested from *C. trachomatis*-infected HeLa cell monolayers by scraping 3
1121 wells of a 6-well plate in ice-cold PBS + 10% Proteinase K (ThermoFisher Scientific).
1122 Samples were then pooled and split into two technical replicates for analysis of genome
1123 copy number by qPCR. gDNA was isolated using the DNeasy Blood and Tissue Kit
1124 following manufacturer protocols (QIAGEN, Hilden, Germany). gDNA was stored at -20°
1125 C until further use.
1126
1127 **Reverse Transcription Quantitative Polymerase Chain Reaction (RT-qPCR)**
1128 cDNA (or gDNA in qPCR), prepared as described above, was diluted 1:10 or 1:100 in
1129 nuclease-free H_2O depending on the experimental condition being assayed (*e.g.*
1130 treatment, point in development cycle, etc.). On ice, 3.3 μL of diluted sample was added
1131 to 79 μL of PowerUp™ SYBR® Green Master Mix (ThermoFisher Scientific) with
1132 specific qPCR primers diluted to 500 nM. From this master mix, each experimental
1133 sample was assayed in triplicate 25 μL reactions. Assays were run on an Applied
1134 Biosystems 7300 Real Time PCR System with cycling conditions as follows: Stage 1:
1135 50.0° C for 2 min, 1 rep. Stage 2: 95.0° C for 10 min, 1 rep. Stage 3: 95.0° C for 15 sec,
1136 40 reps. Stage 4: 60.0° C for 1 min, 1 rep. Primers were subjected to dissociation curve
1137 analysis to ensure that a single product was generated. For each primer set, a standard
1138 curve was generated using purified *C. trachomatis* L2 gDNA from EB preparations
1139 diluted from 2 x 10^{-3} to 2 x10^{0} ng per reaction. Ct values generated from each
1140 experimental reaction were then fit to standard curves (satisfying an efficiency of
1141 95±5%) for the respective primer pair and from the calculated ng quantities, transcript or
1142 genome copy number was calculated as follows:
1143

1144 $$Genome\ copy\ number\ \left(\frac{genome\ copies}{ng\ total\ gDNA}\right) = \frac{ng\ genome\ \times\ df}{ng\ total\ gDNA} \times \frac{892{,}000\ copies}{ng\ DNA}$$

1145

1146 $$Transcript\ copy\ number\ \left(\frac{transcript\ copies}{\frac{genome\ copies}{ng\ total\ gDNA}}\right) = \frac{ng\ transcript\ \times\ df}{\frac{genome\ copies}{ng\ total\ gDNA}} \times \frac{892{,}000\ copies}{ng\ DNA}$$

1147
1148 Where *df* = dilution factor and the number of copies/ng DNA is calculated based on the
1149 size of the *C. trachomatis* L2 genome assuming that the molar mass per base pair is
1150 650 (g/mol)/bp (note that this value should be the same for any single-copy ORF on the
1151 genome). All quantifications of genome copy number were determined using the *ahpC*

1152 qPCR primer set. Values from replicate assays were averaged, and values from
1153 replicate RNA/gDNA isolations were averaged to obtain the mean and standard
1154 deviation for one biological replicate. For some experiments, to account for batch effects
1155 across biological replicates, data was transformed such that the mean of all samples in
1156 each replicate was identical. In some instances, batch correcting generated negative
1157 values, and in this case data sets were scaled such that the lowest value equaled 1.0.
1158 HeLa cells were infected at an MOI of 2 for all RT-qPCR studies.
1159
1160 **5' Rapid Amplification of cDNA Ends (5'-RACE)**
1161 All RACE studies were performed using the SMARTer® RACE 5'/3' Kit (Takara Bio). To
1162 observe 5'-RACE products from the *trpRBA* operon, a "nested" RACE protocol was
1163 used as outlined in the SMARTer® RACE 5'/3' Kit user manual. Briefly, 1.25-2.5 μL of
1164 cDNA generated for RACE was added to a 25 μL reaction volume and run in a thermal
1165 cycler for 40 cycles using the touch-down PCR conditions described by the
1166 manufacturer. In brief, 5 cycles were run at an annealing temperature of both 72° C and
1167 70° C prior to 30 cycles run with an annealing temperature of 68° C. Following this
1168 primary amplification, the RACE products were diluted 1:50 in Tricine-EDTA Buffer
1169 supplied by the manufacturer, and 2.5 μL of diluted primary RACE product was added
1170 to a 25 μL reaction volume and subjected to another 20 cycles of nested PCR, as
1171 described by the manufacturer, using primers designed within the amplicon of the
1172 primary RACE products. Samples were electrophoresed on a 2% agarose gel for
1173 visualization and analysis. HeLa cells were infected at a MOI of 5 for all RACE studies.
1174
1175 **3' Rapid Amplification of cDNA Ends (3'-RACE)**
1176 3'-RACE studies were performed essentially identical to 5'-RACE with the exception
1177 that total RNA was subjected to poly(A) tailing with a Poly(A) Polymerase following
1178 manufacturer instructions (New England Biolabs, Ipswich, MA, USA). In brief, at least
1179 3.5 μg of total RNA was incubated at 37° C with Poly(A) Polymerase in reaction buffer
1180 supplemented with ATP and murine RNase Inhibitor (New England Biolabs) for 30
1181 minutes prior to heat-inactivation at 65° C for 20 minutes. RNA was re-isolated through
1182 an RNA clean-up filter cartridge (Ambion, ThermoFisher Scientific). A total of 125 ng of
1183 poly(A)-tailed total RNA was then used to generate 3'-RACE ready cDNA in a 10 μL
1184 reaction volume following manufacturer instructions. Primary and nested RACE was
1185 performed using 3'-RACE gene-specific primers following the same protocol for
1186 amplification described for 5'-RACE, with the exception that the extension time was
1187 adjusted to accommodate amplification of the full ~3 kb *trpRBA* polycistronic message.
1188
1189 **Mapping of 5'/3'-RACE Products**
1190 5'-RACE products generated from either primary or nested RACE reactions were
1191 excised from the agarose gel and DNA was isolated using the NucleoSpin Gel and PCR
1192 Clean-up kit (Macherey-Nagel, Takara Bio). The isolated RACE products were then
1193 cloned into the pRACE vector supplied in the SMARTer® RACE 5'/3' Kit using the In-
1194 Fusion HD cloning kit (Takara Bio). Ligated vectors were transformed into chemically
1195 competent Stellar™ *E. coli* cells by heat shock. Transformed bacteria were plated on LB
1196 agar containing 50 μg/mL carbenicillin and incubated overnight at 37° C. Colonies were
1197 selected and screened for relevant inserts by PCR. Positive colonies were cultured

1198 overnight at 37° C in LB liquid broth containing 50 μg/mL carbenicillin and plasmids
1199 were isolated using the QIAprep Spin Miniprep kit (QIAGEN). Inserts were then
1200 sequenced by Eurofins Genomics using the default M13 Reverse sequencing primer.
1201 Returned sequencing data was aligned to the *C. trachomatis* L2 (434/Bu) genome
1202 (NCBI Accession: NC_010287) by BLAST and the most 5' aligned nucleotide was
1203 considered the 5' end of the insert. In the case of 3'-RACE data, the reverse
1204 complement sequence was first generated prior to alignment. Grouping of individual
1205 products was determined 1.) by clusters being greater than 30 nucleotides apart and 2.)
1206 by the specific RACE band that the alignment was derived from. These two criteria were
1207 not both satisfied in all cases and in those cases criteria 1.) was favored.
1208
1209 **Sequence Alignments**
1210 All *C. trachomatis* L2 434/Bu genome sequences were obtained from NCBI Accession
1211 NC_010287. Global pairwise sequence alignments were made using the EMBOSS
1212 Needle algorithm. Alignment parameters were set as follows: Matrix: DNAfull, Gap
1213 Open: 20, Gap Extend: 0.8, Output Format: pair, End Gap Penalty: True, End Gap
1214 Open: 10, End Gap Extend: 0.5. These conditions were sufficient to replicate the
1215 previously published alignment between the putative YtgR operator sequence and the
1216 TroR operator (Akers et al., 2011). Local pairwise sequence alignments were made
1217 using the EMBOSS Water algorithm. The putative YtgR operator was aligned to the
1218 entire 348 bp intergenic region of the *trpRBA* operon (*C. trachomatis* L2 [434/Bu]
1219 genome position 511,692-512,039). The alignment parameters were set as follows:
1220 Matrix: DNAfull, Gap Open:10, Gap Extend: 0.5, Output Format: pair. These are the
1221 default conditions and were chosen to remove bias from the alignment results.
1222
1223 **Two-Plasmid Reporter Assay**
1224 The YtgR-binding reporter assay was performed essentially as described, with minor
1225 modifications (Thompson et al., 2012). Promoter regions of interest were amplified from
1226 the *C. trachomatis* L2 (434/Bu) genome by PCR using the indicated primer sets, which
1227 included KpnI restriction endonuclease sites at the 5' and 3' ends of the promoter
1228 amplicon. The amplified fragments and the pCCT-EV plasmid were then KpnI-digested
1229 and the promoters ligated into the vector using T4 or Quick Ligase (New England
1230 BioLabs). Insert directionality was confirmed by directional colony PCR and positive
1231 clones were sequence verified. pCCT-*trpBA*ΔOperator was cloned by amplifying two
1232 fragments of the pCCT-*trpBA* vector with one ~60mer primer containing the bases to be
1233 substituted for each fragment. Thus, the whole vector was split into two half-fragments
1234 containing the substituted bases. The two fragments were then cloned back together
1235 using In-Fusion Homology-Directed cloning (Takara Bio) to yield the final vector.
1236 Electrocompetent BL21(DE3) *E. coli* (Sigma Aldrich) were co-transformed by
1237 electroporation with the pCCT reporter plasmid and the pET151 expression vector (-EV
1238 or –YtgR) and plated on double selective LB agar containing 50 μg/mL carbenicillin and
1239 15 μg/mL tetracycline. Prior to plating of transformed cells, 50 μL of 40 mg/mL X-Gal in
1240 DMSO (EMD Millipore, Burlington, MA, USA) was applied to the plate for colorimetric
1241 determination of β-galactosidase expression. Transformants were incubated overnight
1242 at 37° C. The following evening, blue colonies from each experimental condition were
1243 selected and cultured overnight in LB liquid broth containing 0.2% (*w/v*) D-glucose (for

catabolite repression of expression vectors), 50 μg/mL carbenicillin and 15 μg/mL tetracycline. Cultures were incubated overnight at 37° C. The following morning, overnight cultures were spun down to remove glucose-containing media and sub-cultured in LB liquid broth medium containing 50 μM $FeSO_4$, 50 μg/mL carbenicillin and 15 μg/mL tetracycline to an OD_{600} of 0.45. Cultures were incubated for 1 hour at 37° C and sub-cultured a second time in the same media to an OD_{600} of 0.1. Cultures were returned to the incubator for another hour prior to the addition of 500 μM isopropyl β-D-1-thiogalactopyranoside (IPTG) to induce pET151 expression from the *lac* promoter. Cultures were incubated another hour prior to the addition of 0.2% L-arabinose to induce *lacZ* expression from the *araBAD* promoter. Cultures were incubated a final 2 hours prior to the collection of a 0.1 mL volume of cells for assaying β-galactosidase activity by the Miller Assay (J. H. Miller, 1972). Cell pellets were stored at -80° C prior to being assayed. To assay β-galactosidase activity, cell pellets were first re-suspended in Z-buffer (pH 7.0, 60 mM Na_2HPO_4, 40 mM NaH_2PO_4, 10 mM KCl, 1 mM $MgSO_4$ and 2.7 μL/mL β-mercaptoethanol). 50 μL of 0.1% SDS and 100 μL of chloroform were then added to each sample prior to thorough vortexing. Samples were equilibrated for 5 minutes at 30° C and 200 μL of 4 mg/mL ortho-nitrophenyl-β-galactoside (ONPG) prepared in Phosphate Buffer (pH 7.0, 60 mM Na_2HPO_4, 40 mM NaH_2PO_4) were added to the samples to initiate the reaction. Reactions were stopped by the addition of 500 μL 1 M Na_2CO_3. Absorbance was measured on a FLUOStar Optima plate reader (BMG Labtech, Offenburg, Germany) at 420 nm and Miller Units were calculated as:

$$1000 \times \frac{Abs_{420}}{t \times v \times OD_{final}}$$

Where t = reaction time, v = volume of cells and OD_{final} = OD_{600} at the time of sample collection. It was empirically determined that the subtraction of absorbance at 550 nm had a negligible effect on the calculated value. A blank sample lacking cells was included in each experimental batch and used as a reference for absorbance. For each experimental condition, three independent co-transformed colonies were assayed in technical triplicate. In some instances, significantly high Miller Unit outliers were excluded by Grubb's Test ($p < 0.05$) under the assumption that extreme *lacZ* expression may reflect plasmid copy number or reporter gene expression issues.

RNA-Sequencing

RNA-Sequencing experiments were performed as described in their original publication (Brinkworth et al., 2018). Coverage maps were generated by mapping all reads across three biological replicates to a single reference file in CLC Genomics Workbench v11. To facilitate easy analysis of IGR boundaries, the *C. trachomatis* L2 434/Bu genome (Accession: NC_010287) was modified to contain annotations for non-operonic intergenic regions, and this genome was used as the reference for read mapping. Read mapping was performed using default settings in CLC Genomics Workbench. Data aggregation in the Reads track was set to aggregate above 1bp.

Graphs and Statistical Analysis

1288 All graphs were generated using the ggplot2 package (Wickham, 2009) in R Studio, in
1289 Excel and/or in the Adobe Creative Suite. All line plots and bar graphs represent the
1290 mean ± one standard deviation unless otherwise noted. All box and whisker plots
1291 represent the distribution of data between the 1st and 3rd quartile range within the box,
1292 while the whiskers represent data within 1.5 interquartile ranges of the 1st or 3rd quartile.
1293 Extreme values outside this range are plotted as open circles. The 2nd quartile (median)
1294 is plotted as a black line within the box. Histogram plots were generated with a bin width
1295 of 20 and are plotted on a density scale. The overlaid density plots represent a
1296 statistical approximation of the data over a continuous scale. All statistical analyses
1297 were carried out in R Studio. All statistical computations were performed on the mean
1298 values of independent biological replicates calculated from the indicated number of
1299 respective technical replicates. For single pairwise comparisons, a two-sided unpaired
1300 Student's *t*-test with Welch's correction for unequal variance was used to determine
1301 statistical significance. For multiple pairwise comparisons, a One-Way Analysis of
1302 Variance (ANOVA) was conducted to identify significant differences within groups. If a
1303 significant difference was detected, then the indicated post-hoc pairwise test was used
1304 to identify the location of specific statistical differences. A *p*-value less than 0.05 was
1305 considered statistically significant. For all figures, * = $p < 0.05$, ** = $p < 0.01$, and *** = p
1306 < 0.005.
1307

1308 **Acknowledgements.** We thank Liam Caven, Korinn Murphy and Matthew Romero for
1309 critical review of this manuscript; Dr. Christopher C. Thompson for the establishment of
1310 the *E. coli* YtgR reporter system and generation of the pCCT construct; Dr. Scot P.
1311 Ouellette for support, critical feedback and advice; and Dr. David Dewitt for expert
1312 advice, training and maintenance of equipment in the IPN Advanced Imaging Center.
1313 This work was supported by NIH grants R01-AI065545 to R.A.C.; 1F31AI136295 and
1314 5T32GM008336 to N.D.P.; N.D.P. was also supported by an Achievement Reward for
1315 College Scientists (ARCS; Seattle Chapter) Fellowship.

1316 **References**

1317 AbdelRahman, Y. M., & Belland, R. J. (2005). The chlamydial developmental cycle.
1318 *FEMS Microbiology Reviews*, *29*(5), 949–959.
1319 http://doi.org/10.1016/j.femsre.2005.03.002
1320 Akers, J. C., HoDac, H., Lathrop, R. H., & Tan, M. (2011). Identification and functional

1321 analysis of CT069 as a novel transcriptional regulator in Chlamydia. *Journal of*
1322 *Bacteriology*, *193*(22), 6123–6131. http://doi.org/10.1128/JB.05976-11
1323 Akers, J. C., & Tan, M. (2006). Molecular mechanism of tryptophan-dependent
1324 transcriptional regulation in Chlamydia trachomatis. *Journal of Bacteriology*,
1325 *188*(12), 4236–4243. http://doi.org/10.1128/JB.01660-05
1326 Belland, R. J., Nelson, D. E., Virok, D., Crane, D. D., Hogan, D., Sturdevant, D., …
1327 Caldwell, H. D. (2003). Transcriptome analysis of chlamydial growth during IFN-
1328 gamma-mediated persistence and reactivation. *Proceedings of the National*
1329 *Academy of Sciences of the United States of America*, *100*(26), 15971–15976.
1330 http://doi.org/10.1073/pnas.2535394100
1331 Brinkworth, A. J., Wildung, M. R., & Carabeo, R. A. (2018). Genomewide Transcriptional
1332 Responses of Iron-Starved Chlamydia trachomatis Reveal Prioritization of
1333 Metabolic Precursor Synthesis over Protein Translation. *MSystems*, *3*(1), e00184-
1334 17.
1335 Brown, S. A., Palmer, K. L., & Whiteley, M. (2008). Revisiting the host as a growth
1336 medium. *Nature Reviews Microbiology*, *6*(9), 657–666.
1337 http://doi.org/10.1038/nrmicro1955
1338 Byrd, T. F., & Horwitz, M. A. (1993). Regulation of transferrin receptor expression and
1339 ferritin content in human mononuclear phagocytes: Coordinate upregulation by iron
1340 transferrin and downregulation by interferon gamma. *Journal of Clinical*
1341 *Investigation*, *91*(3), 969–976. http://doi.org/10.1172/JCI116318
1342 Byrd, T., & Horwitz, M. A. (1989). Interferon gamma-activated human monocytes
1343 downregulate transferrin receptors and inhibit the intracellular multiplication of

1344 Legionella pneumophila by limiting the availability of iron. *Journal of Clinical*
1345 *Investigation*, *83*(5), 1457–1465. http://doi.org/10.1172/JCI114038
1346 Byrne, G. I., Lehmann, L. K., & Landry, G. J. (1986). Induction of tryptophan catabolism
1347 is the mechanism for gamma-interferon-mediated inhibition of intracellular
1348 Chlamydia psittaci replication in T24 cells. *Infection and Immunity*, *53*(2), 347–351.
1349 Caldwell, H. D., Kromhout, J., & Schachter, J. (1981). Purification and partial
1350 characterization of the major outer membrane protein of Chlamydia trachomatis.
1351 *Infection and Immunity*, *31*(3), 1161–1176.
1352 Carlson, J. H., Porcella, S. F., Mcclarty, G., & Caldwell, H. D. (2005). Comparative
1353 Genomic Analysis of Chlamydia trachomatis Oculotropic and Genitotropic Strains.
1354 *Infection and Immunity*, *73*(10), 6407–6418. http://doi.org/10.1128/IAI.73.10.6407
1355 Carlson, J. H., Wood, H., Roshick, C., Caldwell, H. D., & McClarty, G. (2006). In vivo
1356 and in vitro studies of Chlamydia trachomatis TrpR:DNA interactions. *Molecular*
1357 *Microbiology*, *59*(6), 1678–1691. http://doi.org/10.1111/j.1365-2958.2006.05045.x
1358 Case, E. D. R., Akers, J. C., & Tan, M. (2011). CT406 encodes a chlamydial ortholog of
1359 NrdR, a repressor of ribonucleotide reductase. *Journal of Bacteriology*, *193*(17),
1360 4396–4404. http://doi.org/10.1128/JB.00294-11
1361 Cassat, J. E., & Skaar, E. P. (2013). Iron in Infection and Immunity. *Cell Host and*
1362 *Microbe*, *13*(5), 509–519. http://doi.org/10.1016/j.chom.2013.04.010
1363 CDC. (2017). *2016 Sexually Transmitted Diseases Surveillance - Chlamydia*. Retrieved
1364 from https://www.cdc.gov/std/stats16/chlamydia.htm
1365 Clarke, I. N. (2011). Evolution of Chlamydia trachomatis. *Annals of the New York*
1366 *Academy of Sciences*, *1230*, 11–18. http://doi.org/10.1111/j.1749-

1367 6632.2011.06194.x
1368 Cohen, M., Britigan, B., French, M., & Bean, K. (1987). Preliminary observations on
1369 lactoferrin secretion in human vaginal mucus: variation during the menstrual cycle,
1370 evidence of hormonal regulation, and implications for infection with Neisseria
1371 gonorrhoeae. *American Journal of Obstetrics and Gynecology*, *157*(5), 1122–1125.
1372 Colin, J., Candelli, T., Porrua, O., Boulay, J., Zhu, C., Lacroute, F., … Libri, D. (2014).
1373 Roadblock termination by reb1p restricts cryptic and readthrough transcription.
1374 *Molecular Cell*, *56*(5), 667–680. http://doi.org/10.1016/j.molcel.2014.10.026
1375 Dill, B. D., Dessus-Babus, S., & Raulston, J. E. (2009). Identification of iron-responsive
1376 proteins expressed by Chlamydia trachomatis reticulate bodies during intracellular
1377 growth. *Microbiology*, *155*(1), 210–219. http://doi.org/10.1099/mic.0.022731-0
1378 Eisenreich, W., Dandekar, T., Heesemann, J., & Goebel, W. (2010). Carbon metabolism
1379 of intracellular bacterial pathogens and possible links to virulence. *Nature Reviews*
1380 *Microbiology*, *8*(6), 401–412. http://doi.org/10.1038/nrmicro2351
1381 Fehlner-Gardiner, C., Roshick, C., Carlson, J. H., Hughes, S., Belland, R. J., Caldwell,
1382 H. D., & McClarty, G. (2002). Molecular basis defining human Chlamydia
1383 trachomatis tissue tropism: A possible role for tryptophan synthase. *Journal of*
1384 *Biological Chemistry*, *277*(30), 26893–26903.
1385 http://doi.org/10.1074/jbc.M203937200
1386 Gollnick, P., Babitzke, P., Antson, A., & Yanofsky, C. (2005). Complexity in regulation of
1387 tryptophan biosynthesis in Bacillus subtilis. *Annual Review of Genetics*,
1388 *39*(October), 47–68. http://doi.org/10.1146/annurev.genet.39.073003.093745
1389 Hafner, L. M. (2015). Pathogenesis of fallopian tube damage caused by Chlamydia

1390 trachomatis infections. *Contraception*, *92*(2), 108–115.
1391 http://doi.org/10.1016/j.contraception.2015.01.004
1392 Hood, M. I., & Skaar, E. P. (2012). Nutritional immunity: Transition metals at the
1393 pathogen-host interface. *Nature Reviews Microbiology*, *10*(8), 525–537.
1394 http://doi.org/10.1038/nrmicro2836
1395 Igietseme, J. U., Ananaba, G. A., Candal, D. H., Lyn, D., & Black, C. M. (1998). Immune
1396 control of Chlamydial growth in the human epithelial cell line RT4 involves multiple
1397 mechanisms that include nitric oxide induction, tryptophan catabolism and iron
1398 deprivation. *Microbiology and Immunology*, *42*(9), 617–625.
1399 Kelver, M. E., Kaul, A., Nowicki, B., Findley, W. E., Hutchens, T. W., & Nagamani, M.
1400 (1996). Estrogen regulation of lactoferrin expression in human endometrium.
1401 *American Journal of Reproductive Immunology*, *36*(5), 243–247.
1402 Lloyd, J. M., O'Dowd, T., Driver, M., & Tee, D. E. (1984). Demonstration of an epitope of
1403 the transferrin receptor in human cervical epithelium--a potentially useful cell
1404 marker. *Journal of Clinical Pathology*, *37*(2), 131–135. Retrieved from
1405 http://www.ncbi.nlm.nih.gov/entrez/query.fcgi?cmd=Retrieve&db=PubMed&dopt=Ci
1406 tation&list_uids=6198338
1407 Macchiarulo, A., Camaioni, E., Nuti, R., & Pellicciari, R. (2009). Highlights at the gate of
1408 tryptophan catabolism : a review on the mechanisms of activation and regulation of
1409 indoleamine 2,3-dioxygenase (IDO), a novel target in cancer disease. *Amino Acids*,
1410 *37*, 219–229. http://doi.org/10.1007/s00726-008-0137-3
1411 Merino, E., & Yanofsky, C. (2005). Transcription attenuation: A highly conserved
1412 regulatory strategy used by bacteria. *Trends in Genetics*, *21*(5), 260–264.

1413 http://doi.org/10.1016/j.tig.2005.03.002
1414 Miller, J. D., Sal, M. S., Schell, M., Whittimore, J. D., & Raulston, J. E. (2009).
1415 Chlamydia trachomatis YtgA is an iron-binding periplasmic protein induced by iron
1416 restriction. *Microbiology*, *155*(9), 2884–2894. http://doi.org/10.1099/mic.0.030247-0
1417 Miller, J. H. (1972). Assay of β-galactosidase. In *Experiments in Molecular Genetics*.
1418 Cold Spring Harbor Laboratory Press.
1419 Moore, E. R., & Ouellette, S. P. (2014). Reconceptualizing the chlamydial inclusion as a
1420 pathogen-specified parasitic organelle: an expanded role for Inc proteins. *Frontiers*
1421 *in Cellular and Infeciton Microbiology*, *4*(October), 1–10.
1422 http://doi.org/10.3389/fcimb.2014.00157
1423 Mueller, K. E., Wolf, K., & Fields, K. A. (2016). Gene Deletion by Fluorescence-
1424 Reported Allelic Exchange Mutagenesis in Chlamydia trachomatis. *MBio*, *7*(1), 1–9.
1425 http://doi.org/10.1128/mBio.01817-15.Invited
1426 Nairz, M., Fritsche, G., Brunner, P., Talasz, H., Hantke, K., & Weiss, G. (2008).
1427 Interferon-γ limits the availability of iron for intramacrophage Salmonella
1428 typhimurium. *European Journal of Immunology*, *38*(7), 1923–1936.
1429 http://doi.org/10.1002/eji.200738056
1430 Nelson, D. E., Virok, D. P., Wood, H., Roshick, C., Johnson, R. M., Whitmire, W. M., …
1431 Caldwell, H. D. (2005). Chlamydial IFN-gamma immune evasion is linked to host
1432 infection tropism. *Proceedings of the National Academy of Sciences of the United*
1433 *States of America*, *102*(30), 10658–63. http://doi.org/10.1073/pnas.0504198102
1434 Newman, L., Rowley, J., Hoorn, S. Vander, Wijesooriya, N. S., Unemo, M., Low, N., …
1435 Temmerman, M. (2015). Global Estimates of the Prevalence and Incidence of Four

1436 Curable Sexually Transmitted Infections in 2012 Based on Systematic Review and
1437 Global Reporting. *PLoS ONE*, *10*(12), 1–17.
1438 http://doi.org/10.1371/journal.pone.0143304
1439 Nogueira, A. T., Braun, K. M., & Carabeo, R. A. (2017). Characterization of the Growth
1440 of Chlamydia trachomatis in In Vitro-Generated Stratified Epithelium. *Frontiers in*
1441 *Cellular and Infection Microbiology*, *7*(October), 1–16.
1442 http://doi.org/10.3389/fcimb.2017.00438
1443 Østergaard, O., Follmann, F., Olsen, A. W., Heegaard, N. H., Andersen, P., &
1444 Rosenkrands, I. (2016). Quantitative Protein Profiling of Chlamydia trachomatis
1445 Growth Forms Reveals Defense Strategies Against Tryptophan Starvation.
1446 *Molecular & Cellular Proteomics : MCP*, *15*(12), 3540–3550.
1447 http://doi.org/10.1074/mcp.M116.061986
1448 Ouellette, S. P. (2018). Feasibility of a Conditional Knockout System for Chlamydia
1449 Based on CRISPR Interference. *Frontiers in Cellular and Infection Microbiology*,
1450 *8*(February). http://doi.org/10.3389/fcimb.2018.00059
1451 Ouellette, S. P., & Carabeo, R. A. (2010). A functional slow recycling pathway of
1452 transferrin is required for growth of Chlamydia. *Frontiers in Microbiology*, *1*(OCT),
1453 1–12. http://doi.org/10.3389/fmicb.2010.00112
1454 Ouellette, S. P., Rueden, K. J., & Rucks, E. A. (2016). Tryptophan codon-dependent
1455 transcription in chlamydia pneumoniae during gamma interferon-mediated
1456 tryptophan limitation. *Infection and Immunity*, *84*(9), 2703–2713.
1457 http://doi.org/10.1128/IAI.00377-16
1458 Pokorzynski, N. D., Thompson, C. C., & Carabeo, R. A. (2017). Ironing Out the

1459 Unconventional Mechanisms of Iron Acquisition and Gene Regulation in
1460 Chlamydia. *Frontiers in Cellular and Infection Microbiology*, *7*(September), 1–19.
1461 http://doi.org/10.3389/fcimb.2017.00394
1462 Raulston, J. E. (1997). Response of Chlamydia trachomatis serovar E to iron restriction
1463 in vitro and evidence for iron-regulated chlamydial proteins. *Infection and Immunity*,
1464 *65*(11), 4539–4547.
1465 Raulston, J. E., Miller, J. D., Davis, C. H., Schell, M., Baldwin, A., Ferguson, K., & Lane,
1466 H. (2007). Identification of an iron-responsive protein that is antigenic in patients
1467 with Chlamydia trachomatis genital infections. *FEMS Immunology and Medical*
1468 *Microbiology*, *51*(3), 569–576. http://doi.org/10.1111/j.1574-695X.2007.00336.x
1469 Ray, K., Marteyn, B., Sansonetti, P. J., & Tang, C. M. (2009). Life on the inside: The
1470 intracellular lifestyle of cytosolic bacteria. *Nature Reviews Microbiology*, *7*(5), 333–
1471 340. http://doi.org/10.1038/nrmicro2112
1472 Ricci, S., Ratti, G., & Scarlato, V. (1995). Transcriptional regulation in the Chlamydia
1473 trachomatis pCT plasmid. *Gene*, *154*(1), 93–98. http://doi.org/10.1016/0378-
1474 1119(94)00825-D
1475 Sasaki-Imamura, T., Yoshida, Y., Suwabe, K., Yoshimura, F., & Kato, H. (2011).
1476 Molecular basis of indole production catalyzed by tryptophanase in the genus
1477 Prevotella. *FEMS Microbiology Letters*, *322*(1), 51–59.
1478 http://doi.org/10.1111/j.1574-6968.2011.02329.x
1479 Schindelin, J., Arganda-Carreras, I., Frise, E., Kaynig, V., Longair, M., Pietzsch, T., …
1480 Cardona, A. (2012). Fiji: An open-source platform for biological-image analysis.
1481 *Nature Methods*, *9*(7), 676–682. http://doi.org/10.1038/nmeth.2019

1482 Schmitt, M. P. (2002). Analysis of a DtxR-Like Metalloregulatory Protein, MntR, from
1483 Corynebacterium diphtheriae That Controls Expression of an ABC Metal
1484 Transporter by an Mn(2+)-Dependent Mechanism. *Journal of Bacteriology*, *184*(24),
1485 6882–6892. http://doi.org/10.1128/JB.184.24.6882
1486 Seth-Smith, H. M. B., Harris, S. R., Persson, K., Marsh, P., Barron, A., Bignell, A., …
1487 Clarke, I. N. (2009). Co-evolution of genomes and plasmids within Chlamydia
1488 trachomatis and the emergence in Sweden of a new variant strain. *BMC Genomics*,
1489 *10*, 239. http://doi.org/10.1186/1471-2164-10-239
1490 Skaar, E. P. (2010). The battle for iron between bacterial pathogens and their vertebrate
1491 hosts. *PLoS Pathogens*, *6*(8), 1–2. http://doi.org/10.1371/journal.ppat.1000949
1492 Spear, G. T., Kendrick, S. R., Chen, H. Y., Thomas, T. T., Bahk, M., Balderas, R., …
1493 Landay, A. L. (2011). Multiplex immunoassay of lower genital tract mucosal fluid
1494 from women attending an urban STD clinic shows broadly increased IL1ß and
1495 lactoferrin. *PLoS ONE*, *6*(5), 1–7. http://doi.org/10.1371/journal.pone.0019560
1496 Stephens, R. S., Kalman, S., Lammel, C., Fan, J., Marathe, R., Aravind, L., …
1497 Gunderson, J. H. (1998). Genome sequence of an obligate intracellular pathogen of
1498 humans: Chlamydia trachomatis. *Science*, *282*(5389), 754–759.
1499 http://doi.org/10.1126/science.282.5389.754
1500 Tao, X., Boydt, J., & Murphy, J. R. (1992). Specific binding of the diphtheria tox
1501 regulatory element DtxR to the tox operator requires divalent heavy metal ions and
1502 a 9-base-pair interrupted palindromic sequence. *Proceedings of the National*
1503 *Academy of Sciences of the United States of America*, *89*(13), 5897–5901.
1504 Taylor, H. R., Burton, M. J., Haddad, D., West, S., & Wright, H. (2014). Trachoma. *The*

1505 *Lancet*, *384*(9960), 2142–2152. http://doi.org/10.1016/S0140-6736(13)62182-0
1506 Taylor, M. W., & Feng, G. S. (1991). Relationship between interferon-gamma,
1507 indoleamine 2,3-dioxygenase, and tryptophan catabolism. *FASEB J.*, *5*(11), 2516–
1508 2522. Retrieved from http://www.fasebj.org/cgi/reprint/5/11/2516.pdf
1509 Thompson, C. C., & Carabeo, R. A. (2011). An optimal method of iron starvation of the
1510 obligate intracellular pathogen, Chlamydia trachomatis. *Frontiers in Microbiology*,
1511 *2*(20). http://doi.org/10.3389/fmicb.2011.00020
1512 Thompson, C. C., Nicod, S. S., Malcolm, D. S., Grieshaber, S. S., & Carabeo, R. A.
1513 (2012). Cleavage of a putative metal permease in Chlamydia trachomatis yields an
1514 iron-dependent transcriptional repressor. *Proceedings of the National Academy of*
1515 *Sciences of the United States of America*, *109*(26), 10546–51.
1516 http://doi.org/10.1073/pnas.1201398109
1517 Thomson, N. R., Holden, M. T. G., Carder, C., Lennard, N., Lockey, S. J., Marsh, P., …
1518 Clarke, I. N. (2008). Chlamydia trachomatis : Genome sequence analysis of
1519 lymphogranuloma venereum isolates. *Genome Research*, *18*(1), 161–171.
1520 http://doi.org/10.1101/gr.7020108.
1521 Valenti, P., Rosa, L., Capobianco, D., Lepanto, M. S., Schiavi, E., Cutone, A., …
1522 Mastromarino, P. (2018). Role of Lactobacilli and Lactoferrin in the Mucosal
1523 Cervicovaginal Defense. *Frontiers in Immunology*, *9*(March), 1–14.
1524 http://doi.org/10.3389/fimmu.2018.00376
1525 Wickham, H. (2009). *ggplot2: Elegant Graphics for Data Analysis.* Springer-Verlag New
1526 York.
1527 Wood, H., Fehlner-Gardner, C., Berry, J., Fischer, E., Graham, B., Hackstadt, T., …

McClarty, G. (2003). Regulation of tryptophan synthase gene expression in Chlamydia trachomatis. *Molecular Microbiology*, *49*(5), 1347–1359. http://doi.org/10.1046/j.1365-2958.2003.03638.x

Wood, H., Roshick, C., & McClarty, G. (2004). Tryptophan recycling is responsible for the interferon-? resistance of Chlamydia psittaci GPIC in indoleamine dioxygenase-expressing host cells. *Molecular Microbiology*, *52*(3), 903–916. http://doi.org/10.1111/j.1365-2958.2004.04029.x

Wyrick, P. B. (2010). Chlamydia trachomatis Persistence In Vitro: An Overview. *The Journal of Infectious Diseases*, *201*, 88–95. http://doi.org/10.1086/652394

Yanofsky, C. (1981). Attenuation in the control of expression of bacterial operons. *Nature*, *289*(5800), 751–758. http://doi.org/10.1038/289751a0

Ziklo, N., Huston, W. M., Hocking, J. S., & Timms, P. (2016). Chlamydia trachomatis Genital Tract Infections: When Host Immune Response and the Microbiome Collide. *Trends in Microbiology*, *24*(9), 750–765. http://doi.org/10.1016/j.tim.2016.05.007

Author Contributions: N.D.P. and R.A.C. wrote the manuscript; A.J.B. and R.A.C. designed and analyzed data for the RNA-Sequencing experiments; A.J.B. performed RNA-Seq experiments; N.D.P. and R.A.C. re-analyzed the RNA-Sequencing data for this publication; N.D.P. and R.A.C. designed all other experiments; N.D.P. performed all other experiments; N.D.P. and R.A.C. analyzed and interpreted the data for all other experiments.

Supplementary Figures

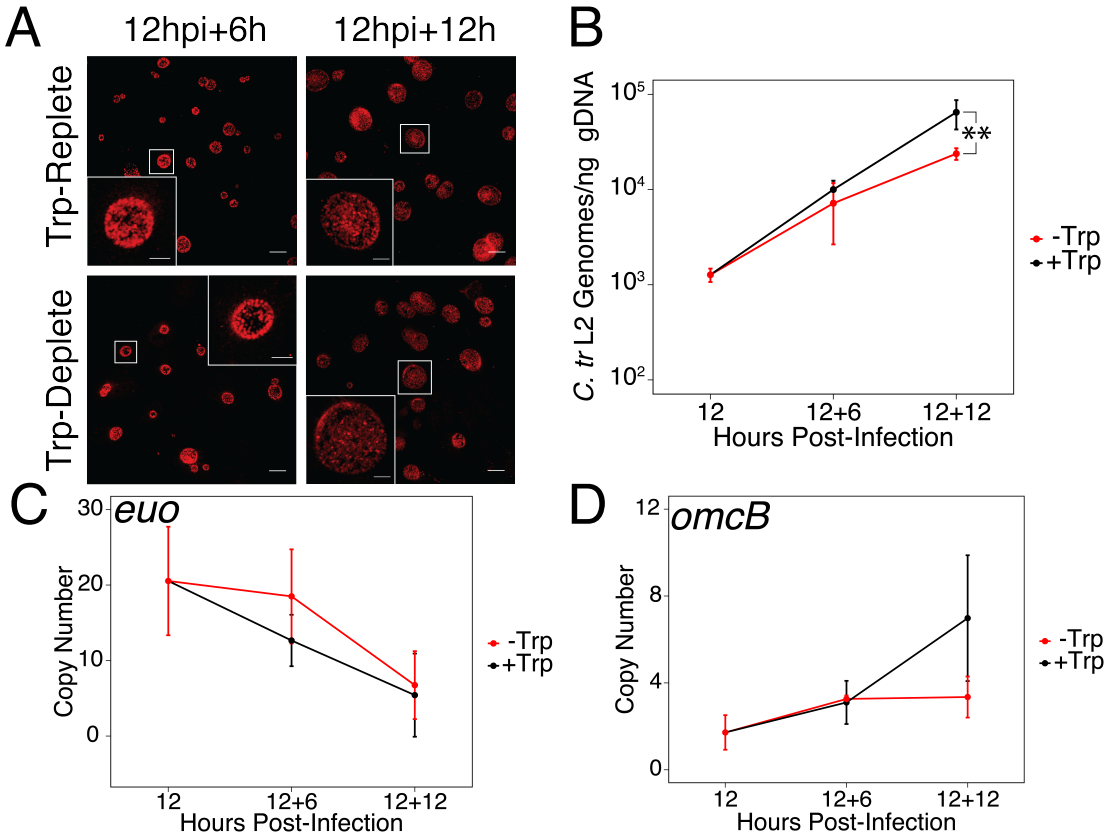

Figure 1 – Figure Supplement 1. Brief media-defined tryptophan limitation does not produce characteristically persistent *Chlamydia.* (*A*) *C. trachomatis* L2-infected HeLa cells were fixed and stained with convalescent human sera to image inclusion morphology by confocal microscopy following tryptophan limitation at the indicated times post-infection. Figure shows representative experiment of two biological replicates. Scale bar = 15 μm, Inset scale bar = 5 μm. (*B*) Genomic DNA (gDNA) was harvested from infected HeLa cells at the indicated times post-infection under tryptophan-replete (black) and -deplete (red) conditions. Chlamydial genome copy number was quantified by qPCR. Chlamydial genome replication is stalled following 12 hours of tryptophan limitation, but not 6. N=2. (*C*) Total RNA was harvested from infected HeLa cells at the indicated times post-infection under tryptophan-replete (black) and -deplete (red) conditions. The transcript abundance of hallmark persistence genes *euo* and (*D*) *omcB* were quantified by RT-qPCR and normalized against genome copy number. No period of tryptophan limitation significantly impacted *euo* or *omcB* expression. N=2. Statistical significance was determined by One-Way ANOVA followed by post-hoc pairwise *t*-tests with Bonferroni's correction for multiple comparisons.

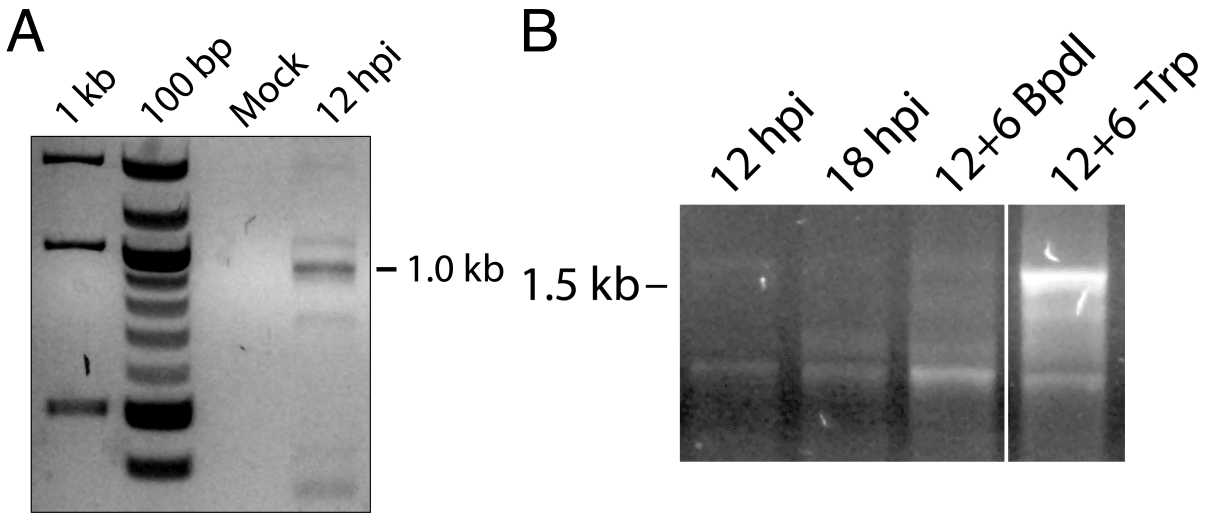

Figure 4 – Figure Supplement 1. 5'-RACE conditions produce *Chlamydia*-specific products that are amplified in primary RACE. (*A*) Total RNA harvested from mock-infected HeLa cells was processed for 5'-RACE in parallel with infected samples to determine specificity of amplified products to *Chlamydia*-infected cells. No RACE products were detected in the mock-infected sample. (*B*) Primary products amplified from 5'-RACE were electrophoresed on an agarose gel and visualized. Weak bands corresponding to those detected by nested 5'-RACE were observed, with the noted relative abundance of the 1.0 and 1.5 kb products in the Bpdl-treated and Trp-deplete conditions, respectively.

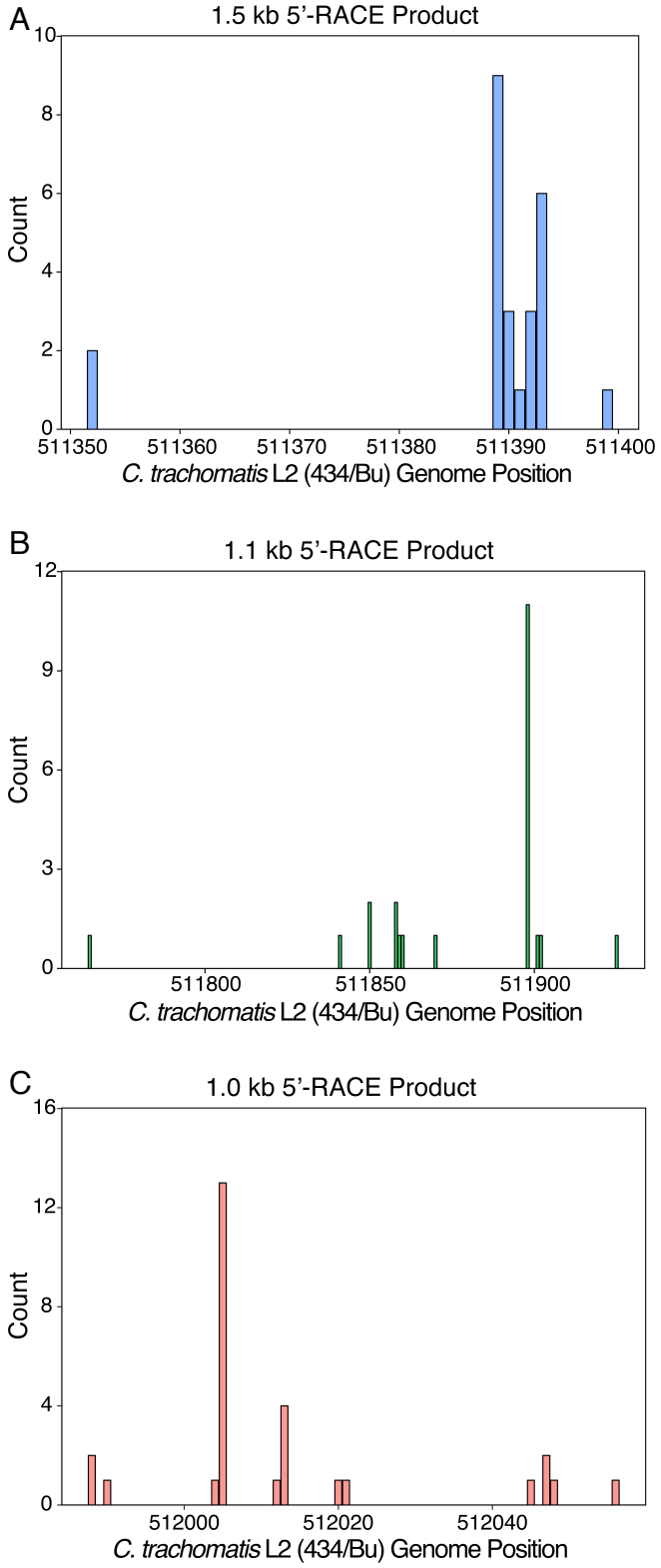

Figure 4 – Figure Supplement 2. Mapping of 5'-RACE products at the individual nucleotide level. (*A*) Mapping of the 1.5 kb 5'-RACE product. (*B*) Mapping of the 1.1 kb 5'-RACE product. (*C*) Mapping of the 1.0 kb 5'-RACE product.

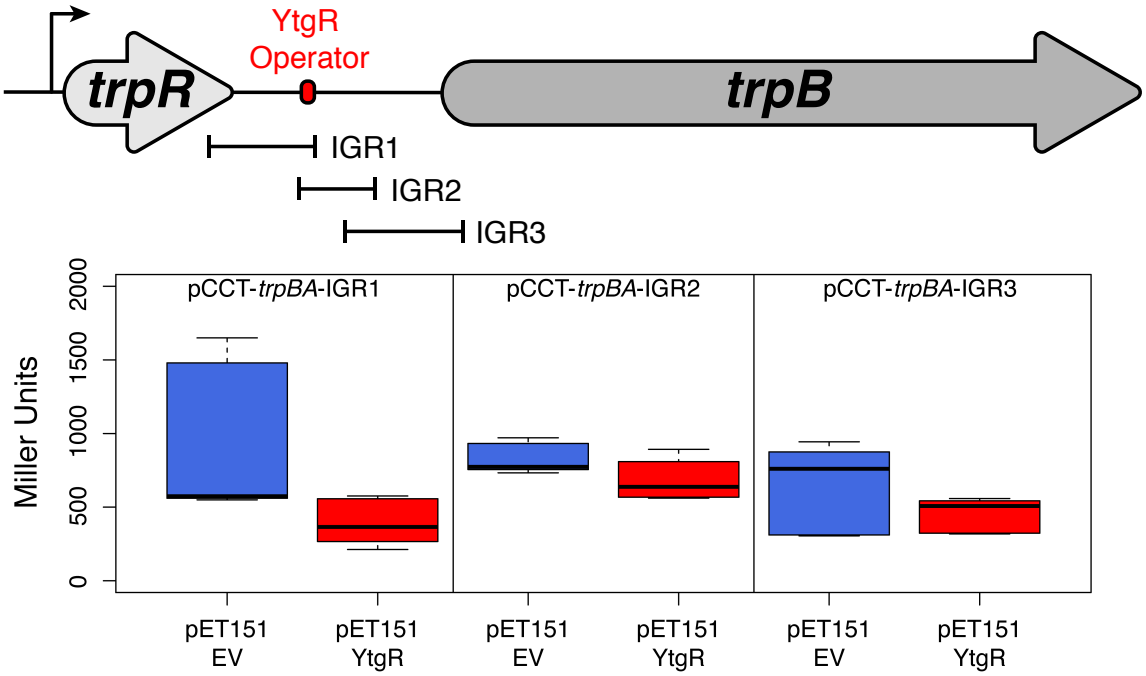

Figure 5 – Figure Supplement 1. Truncated fragments of the *trpRBA* IGR are not sufficient to confer YtgR repression phenotype, regardless of the presence of the putative operator site. The cartoon depiction of the *trpRBA* operon indicates the position of the IGR fragments cloned into each of the reporter vectors (*i.e.* pCCT-IGR1 through IGR3). No statistically meaningful differences were detected in the β-galactosidase activity in the presence of any of the IGR fragments.

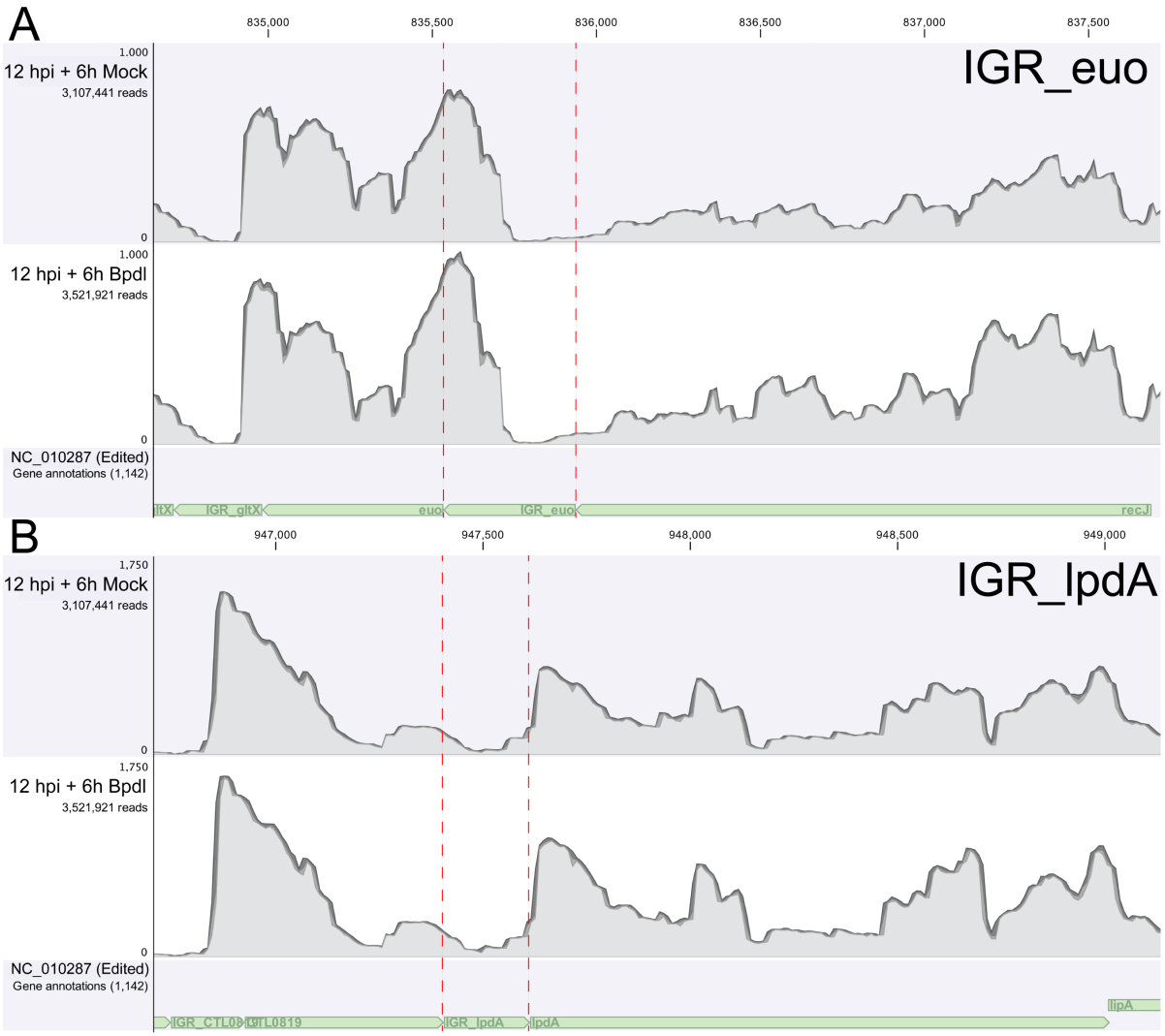

Figure 6 – Figure Supplement 1. RNA-Sequencing coverage map of reads mapping to the intergenic regions upstream of *euo* and *lpdA*. (*A*) Coverage map for the IGR upstream of *euo*, a gene that is neither iron-regulated nor YtgR-regulated. (*B*) Coverage map for the IGR upstream of *lpdA*, a gene that is iron-regulated but not YtgR-regulated. Neither coverage map indicates an increase in reads mapping to these intergenic regions, suggesting that the effect observed at the *trpRBA* IGR is specific.

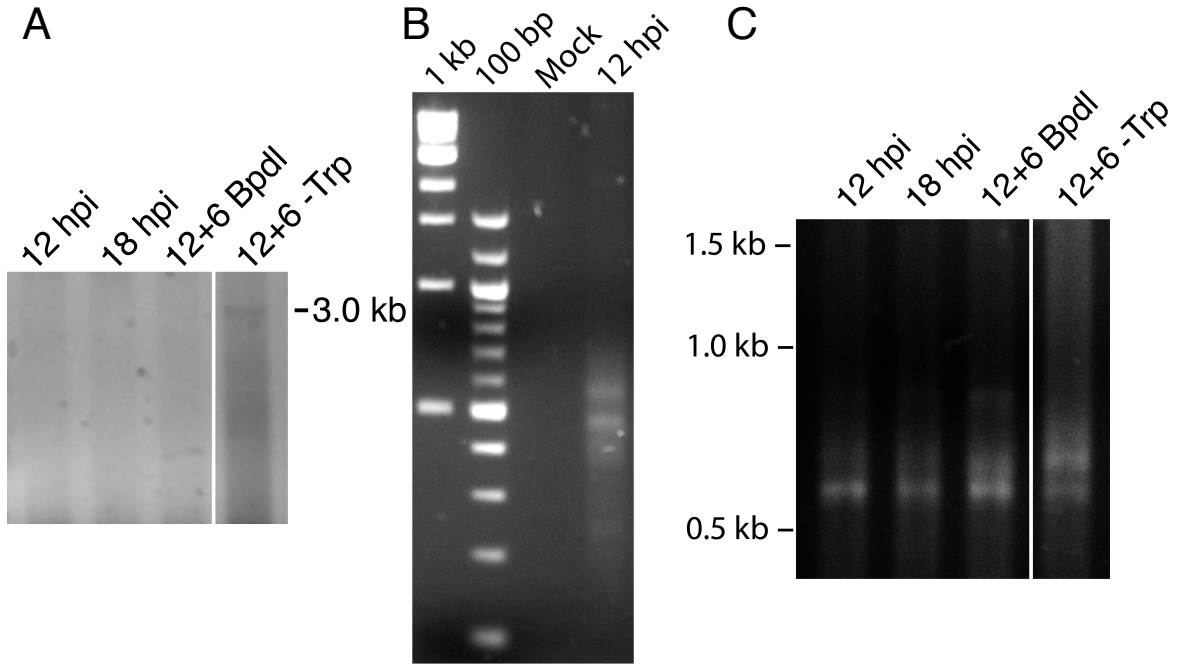

Figure 6 – Figure Supplement 2. 3'-RACE conditions produce *Chlamydia*-specific products that are amplified in primary RACE. (*A*) Contrast-adjusted image to show weak amplification of ~3.0 kb full-length *trpRBA* transcript in nested 3'-RACE reaction. (*B*) Total RNA harvested from mock-infected HeLa cells was processed for 3'-RACE in parallel with infected samples to determine specificity of amplified products to *Chlamydia*-infected cells. No RACE products were detected in the mock-infected sample. (*C*) Primary products amplified from 3'-RACE were electrophoresed on an agarose gel and visualized. Weak bands that were relatively non-specific were detected in the 3'-RACE primary amplification, emphasizing the utility of producing enhanced specificity in the nested amplification.

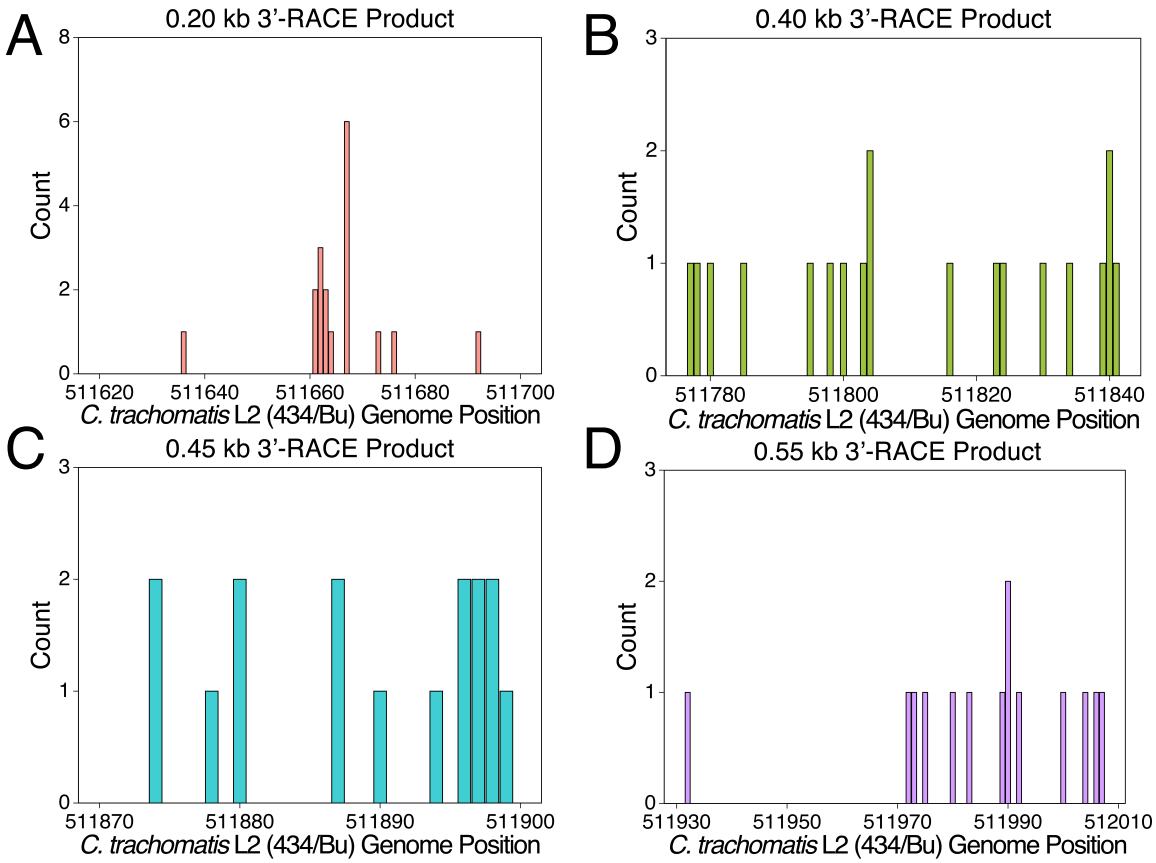

Figure 6 – Figure Supplement 3. Mapping of the 3'-RACE products at the individual nucleotide level. (*A*) Mapping of the 0.20 kb 3'-RACE product. (*B*) Mapping of the 0.40 kb 3'-RACE product. (*C*) Mapping of the 0.45 kb 3'-RACE product. (*D*) Mapping of the 0.55 kb 3'-RACE product.